Geochemistry, Geophysics, Geosystems

RESEARCH ARTICLE
10.1029/2020GC009472

Thallium Isotopes Reveal Brine Activity During Carbonatite Magmatism

Forrest Horton[1], Sune Nielsen[1], Yunchao Shu[1,2], Alan Gagnon[1], and Jerzy Blusztajn[1]

[1]Woods Hole Oceanographic Institution, Woods Hole, MA, USA, [2]University of Science and Technology, Hefei, China

Key Points:

- Thallium isotopes fractionate in carbonatite volcanic systems
- Thallium in carbonatites may derive from recycled ocean crust
- Brines cause potassic metasomatism during ascent and eruption of carbonatite magmas

Correspondence to:
F. Horton,
horton@whoi.edu

Citation:
Horton, F., Nielsen, S., Shu, Y., Gagnon, A., & Blusztajn, J. (2021). Thallium isotopes reveal brine activity during carbonatite magmatism. *Geochemistry, Geophysics, Geosystems*, *22*, e2020GC009472. https://doi.org/10.1029/2020GC009472

Received 9 OCT 2020
Accepted 21 JAN 2021

Abstract Carbonatite volcanism remains poorly understood compared to silicic volcanism due to the scarcity of carbonatite volcanoes worldwide and because volcanic H_2O and CO_2—major components in carbonatite volcanic systems—are not well preserved in the rock record. To further our understanding of carbonatite genesis, we utilize the non-traditional thallium (Tl) isotope system in Khanneshin carbonatites in Afghanistan. These carbonatites contain 250–30,000 ng/g Tl and have ε^{205}Tl values (−4.6 to +4.6) that span much of the terrestrial igneous range. We observe that $\delta^{18}O_{VSMOW}$ (+8.6‰ to +23.5‰) correlates positively with $\delta^{13}C_{VPDB}$ (−4.6‰ to +3.5‰) and ε^{205}Tl up to $\delta^{18}O = 15‰$. Rayleigh fractionation of calcite from an immiscible CO_2-H_2O fluid with a mantle-like starting composition can explain the $\delta^{18}O$ and $\delta^{13}C$—but not ε^{205}Tl—trends. Biotite fractionates Tl isotopes in other magmatic settings, so we hypothesize that a Tl-rich hydrous brine caused potassic metasomatism (i.e., biotite fenitization) of wall rock that increased the ε^{205}Tl of the residual magma-fluid reservoir. Our results imply that, in carbonatitic volcanic systems, simultaneous igneous differentiation and potassic metasomatism increase ε^{205}Tl, $\delta^{18}O$, $\delta^{13}C$, and light rare earth element concentrations in residual fluids. Our fractionation models suggest that the Tl isotopic compositions of the primary magmas were among the isotopically lightest (less than or equal to $\varepsilon^{205}Tl = -4.6$) material derived from the mantle for which Tl isotopic constraints exist. If so, the ultimate source of Tl in Khanneshin lavas—and perhaps carbonatites elsewhere—may be recycled ocean crust.

Plain Language Summary Most volcanoes on Earth are silica-rich. Rare volcanoes that are composed of mostly carbonate minerals (referred to as carbonatite volcanoes) are not as well understood, but provide clues about carbon fluxes into and out of the mantle. To further our understanding of carbonatite genesis, we measured the thallium, oxygen, and carbon isotopes in rocks from a carbonatite volcano in Afghanistan. We discovered systematic variations in all three isotope systems caused by the massive release of carbon dioxide- and water-rich fluids from the magmas prior to eruption. Interaction between these fluids and the surrounding rock—which we argue is fundamental to carbonatite genesis—appears to be largely responsible for magma evolution. As the first study of thallium isotopes in carbonatites, our results also have implications for the origins of carbonatite magmas: we infer that the magmas initially had thallium isotope compositions most similar to ocean crust, which implies that seafloor thallium cycles deep into the mantle and returns to the surface in carbonatitic magmas.

1. Introduction

Carbonatite and carbonated silicate melts are thought to be widespread in oxidized regions of Earth's upper mantle (Dasgupta, 2013; Hammouda & Keshav, 2015), yet constitute only a minor fraction of the magmas that reach Earth's surface. Because volcanologists have witnessed active eruptions from only one carbonatite volcano—Ol Doinyo Lengai in Tanzania (Dawson et al., 1990)—our understanding of carbonatite volcanism is largely based on geological observations and experimental constraints. The latter are challenging to obtain because carbonatitic magmas and fluids that exsolve from them are difficult to quench in laboratory settings (e.g., Veksler & Keppler, 2000). Carbonatitic magmas can form by low-degree partial melting of carbonated mantle or by exsolution from, and immiscibility with, alkaline silicate magmas (Gittins, 1988; Hamilton et al., 1979; Wyllie, 1989). Water can be a major constituent of carbonatite magmas: 10 wt.% H_2O is soluble at 1 kbar and even more at higher pressures (Keppler, 2003). Such hydrous carbonatitic fluids are very buoyant relative to ambient mantle (Ritter et al., 2020). Decarbonation reactions between ascending carbonatite magmas and silica-rich wall rocks produce CO_2 when they reach 100-80 km depth (Wyllie &

Huang, 1975). Exsolution of hydrous fluids begins at ~60 km depth (Falloon & Green, 1990), which accelerates magma ascent and prompts further devolatilization. By the time they reach the upper crust, carbonatite magmas potentially lose large volume fractions of carbon (via decarbonation reactions) and H_2O (via exsolution) and have undergone profound geochemical transformations. For these reasons, carbonatite volcanism is distinct from and poorly understood compared to silicic volcanism.

Stable isotopes in carbonatites record a rich and complex devolatilization history. Globally, carbonatites exhibit wide ranges of $\delta^{13}C$ (−8‰ to +2‰) and $\delta^{18}O$ (+5‰ to +30‰) (Keller & Hoefs, 1995; Pineau et al., 1973; Taylor et al., 1967). Mantle isotopic variability (Woolley & Church, 2005) is insufficient to explain the $\delta^{13}C$ and $\delta^{18}O$ ranges observed at individual localities, which typically span much of the global range. In most carbonatite complexes, only the isotopically light $\delta^{13}C$ and $\delta^{18}O$ compositions ($\delta^{13}C$ from −8‰ to −5‰ and $\delta^{18}O$ from +5‰ to +9‰) are thought to represent primary mantle-derived magmas (Taylor et al., 1967). Such values are within the ranges observed in ocean island basalt, midocean ridge basalt (MORB), and kimberlites (Deines & Gold, 1973; Harmon & Hoefs, 1995; Javoy et al., 1986). Thus, deviations from mantle-like $\delta^{13}C$ and $\delta^{18}O$ in carbonatites are thought to reflect pre-, syn-, and post-eruptive processes, including devolatilization, fractional crystallization, and meteoric alteration (Fosu et al., 2020; Pineau et al., 1973; Ray & Ramesh, 2000).

In recent years, non-traditional isotopic studies have placed constraints on carbonatite origins. Boron isotopes indicate that young carbonatites (<300 Ma) contain recycled crustal components, whereas older carbonatites do not (Hulett et al., 2016). Calcium isotopes seem to corroborate the existence of recycled components in carbonatites: With few exceptions globally, carbonatites have low $\delta^{44/40}Ca$ compared to Earth's mantle, which is consistent with recycling of ancient sedimentary carbonate (Amsellem et al., 2020). In this study, we used the non-traditional thallium (Tl) isotope system to look for evidence of recycled crustal components in carbonatites from the Khanneshin volcanic complex in Helmand Province, Afghanistan. For geochemical context, we also measured major and trace elements, as well as $\delta^{13}C$ and $\delta^{18}O$. We discovered Tl isotopic variability that cannot be solely due to crustal recycling. Unexpectedly, the Tl isotope systematics shed light on enigmatic pre-eruptive processes and help resolve longstanding controversies about carbon and oxygen isotopic fractionation in carbonatitic systems. Our results also provide unequivocal evidence for Tl isotopic fractionation in a volcanic setting, which reveals that Tl isotopic heterogeneities in igneous rocks are not necessarily exclusively inherited from recycled ocean crust and sediments (e.g., Blusztajn et al., 2018; Nielsen et al., 2007; Nielson, Rehkamper, Norman et al., 2006).

1.1. Background

Khanneshin carbonatite volcano in southern Afghanistan is unusually well preserved. Although the precise timing of volcanism is unknown, Khanneshin carbonatites are presumed to be Neogene or younger because they erupted through Neogene sedimentary rocks of the Sistan basin (Figure 1), where intersecting regional faults served as magma conduits (Yeremenko et al., 1975). Soviet (Alkhazov et al., 1978; Vikhter et al., 1976; Yeremenko et al., 1975) and U.S. Geologic Survey (Tucker et al., 2011) publications provide detailed descriptions of the volcanic complex. The central vent of the volcano is ~4 km in diameter and rises 700 m above the surrounding desert. The core of the central vent is considered the oldest part of the volcanic complex and mostly consists of subvolcanic coarse-to medium-grained calcite carbonatite (sövite) that contains abundant mica-rich xenoliths, referred to as glimmerites and fenites. Younger ankerite-barite carbonatites ring the sövite core. The boundary between these two main lithologies is diffuse and the ankerite-barite carbonatites along the periphery of the central vent contain many sövite and mica-rich xenoliths. Three stockworks of fine-grained carbonatite (alvikite) later formed on the southeast margin of the central vent; dikes and volcanic plugs of alvikite also exist throughout a volcanic and volcano-sedimentary apron that extends radially 3–5 km from the main vent. Volcanism concluded with three volumetrically minor phonolitic satellite intrusions and subsequent erosion exposed outward dipping Neogene sandstones and siltstones along the margin of the central vent.

Although seemingly a solitary volcanic feature in the Registan desert, as many as eight other minor alkaline igneous centers of similar age may be buried beneath Holocene sands up to 100 km east and west of the Khanneshin carbonatites (Tucker et al., 2011). Unlike most volcano-forming carbonatites (Woolley &

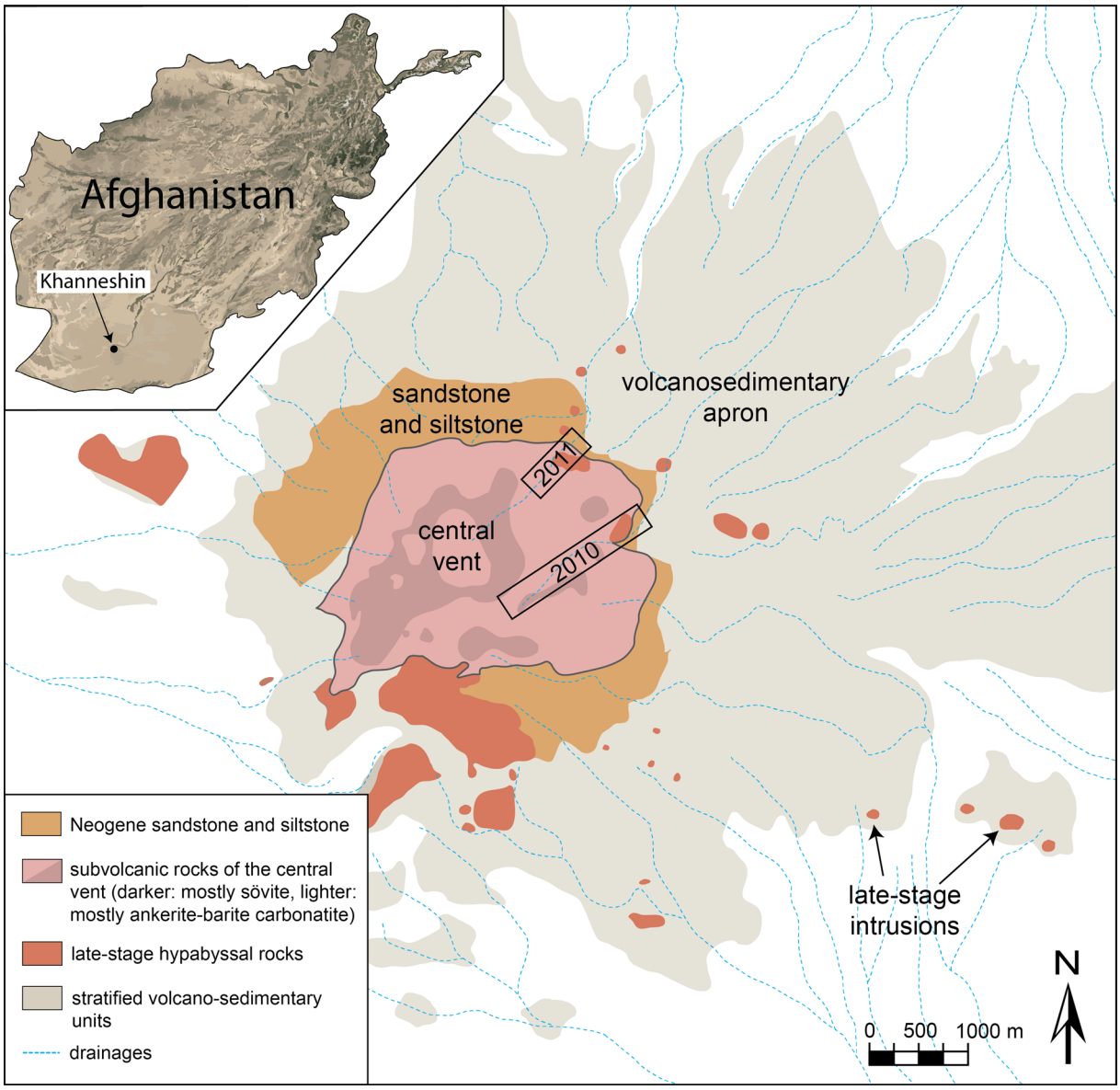

Figure 1. Simplified geologic map of the Neogene Khanneshin volcanic complex, Helmand Province, Afghanistan (modified from Tucker et al., 2011). U.S. Geological Survey, Afghan Geological Survey, and U.S. Department of Defense teams collected samples during 2010 and 2011 missions (rectangles indicate the sampling locations). Carbonatite samples analyzed in this study are from the subvolcanic rocks of the central vent, which erupted through Neogene sandstone and siltstone. Late-stage volcanic plugs and edifices intruded the stratified volcano-sedimentary apron.

Church, 2005), however, there are no voluminous silicate magmatic systems nearby from which Khanneshin magmas may have differentiated. The Sr-Nd-Pb isotopic compositions of Khanneshin rocks are relatively homogenous and distinguish the Khanneshin volcanic complex from carbonatites elsewhere (Ayuso et al., 2013): Pb ($^{206}Pb/^{204}Pb$ = 18.814–18.877, $^{207}Pb/^{204}Pb$ = 15.616–15.674, $^{208}Pb/^{204}Pb$ = 38.892–39.094) and Nd ($^{143}Nd/^{144}Nd$ = 0.512374–0.512462) isotope compositions may represent mixtures of deep mantle Enriched Mantle 1 and high $^{238}U/^{204}Pb$ (HIMU) components (e.g., Zindler & Hart, 1986), whereas the $^{87}Sr/^{86}Sr$ data (0.708034–0.709577) indicate a contribution of Enriched Mantle 2 material, which is typically attributed to ancient subducted sediments or mantle metasomatized by sediment-derived fluids (e.g., Jackson et al., 2007; Workman et al., 2008). These data preclude derivation from MORB mantle.

Soviet geological teams identified the Khanneshin volcanic complex as a potential source of rare earth elements (REEs) in the 1970s. In 2010 and 2011, teams led by the U.S. Geological Survey (USGS) performed

fieldwork to reassess the economic resource potential of the area (Tucker et al., 2011). During a 2010 field mission, a team of geologists accessed the central vent via a drainage on the eastern flank of the massif, collecting samples along a transect from the Neogene sedimentary rocks through the ankerite-barite carbonatite and sövite-rich core of the central vent. A field mission the following year sampled the late-stage REE-rich ankerite-barite carbonatites along the northeastern margin of the central vent. This study examines samples from both localities.

2. Materials and Methods

2.1. Samples

This study investigates 22 rock samples collected during 2010 and 2011 USGS field missions. All except one (a sandstone) were collected from the central vent of the volcano. For simplicity, we classify each of the Khanneshin samples as one of the three lithologies described below. Note that the central vent consists of brecciated fragments of multiple lithologies, so some samples have composite petrologic affinities, even on the thin section scale.

1. *Sandstone*: Khanneshin magmas erupted through Neogene sandstone (FH-10KH-10) that is primarily composed of K-feldspar. Bedding—defined by variable Fe-oxide abundance—was interrupted in places by flame structures prior to sediment consolidation. During magmatism and related metasomatism, calcite and Fe-Mn-oxides precipitated along fracture networks (Figure 2e)
2. *Sövite*: The core of the central vent consists of medium- (KHAN-1) to coarse-grained (RT-10K-9) calcite carbonatite (referred to as sövite) with fine-to coarse-grained biotite (Figures 2a–2c). Accessory phases in the sövites include apatite, strontianite, pyrochlore, and zircon. Tetraferriphlogopite, an unusual Fe-rich mica observed at some carbonatite localities (e.g., Araujo et al., 1998; Lee et al., 2003) and in which Fe plays the structural role of the Al, also exists as a minor phase. These rocks contain two types of xenoliths: (i) glimmerite (Figure 2b) consisting of fine-grained biotite and (ii) fenite (Figure 2c) with K-feldspar cores and biotite rims that range in size from 0.5 mm to 3 m. In places, sövites contain barite-, strontianite-, and apatite-rich veins (Figure 3a). Sample KHAN-3 is distinguished by an abundance of siderite and coarse-grained biotite. RT-10K-12 is a composite sample of sövite and ankerite-barite carbonatite; the sövite portion was targeted for geochemical analyses
3. *Ankerite-barite carbonatite*: The majority of the samples in this study are fine-to medium-grained ferromagnesian carbonatites consisting primarily of ankerite and barite (Figures 2d and 2f). They contain abundant fragments of sövite (RT-10K-12) and glimmerite (RT-11K-6). The ankerite-barite zone along the margins of the central vent consists of an agglomeration of fragments crosscut by veins and dikes. These rocks have variable modal abundances of ankerite, barite, calcite, dolomite, and strontianite. Some have minor biotite, fluorite, magnetite, and/or tetraferriphlogopite. Others contain accessory REE carbonate minerals, including khanneshite ($[Na,Ca]_3[Ba,Sr,Ce,Ca]_3[CO_3]_5$)—for which Khanneshin is the type locality—and bastnäsite ($[REE][CO_3]_3F$), that exist as fine-grained acicular clusters in cavities between calcite and barite (Figure 3d). A subset of the ankerite-barite carbonatites (RT-11K-1, RT-11K-4AO, RT-11K-5A1, RT-11K-5B1A, RT-11K-5B3B, RT-11K-5B4, and RT-11K-5B6C) contains abundant REE carbonate minerals that appear yellow and orange in hand specimens. These rocks were collected in 2011 from decimeter-scale seams that are concentric to the central vent (Tucker et al., 2011)

2.2. Major and Trace Element Geochemistry

Bulk-rock compositions for many of the Khanneshin samples analyzed in this study are reported in Tucker et al. (2011, 2012). To complete the major-element data set, the remaining 13 samples were analyzed with X-ray fluorescent (XRF) spectroscopy at the Washington State University GeoAnalytical Lab, following the protocols described in Johnson et al. (1999). The long-term reproducibility of standards indicates that precision is better than 1% for every major element (1σ). We also analyzed four samples without previous REE determinations via inductively coupled plasma mass spectrometry (ICPMS) at Washington State University GeoAnalytical Lab. Powdered samples were mixed with lithium tetraborate flux and fused at 1000°C in a carbon crucible. The resulting fusion beads were dissolved in HNO_3, HF, and $HClO_4$ solutions that were

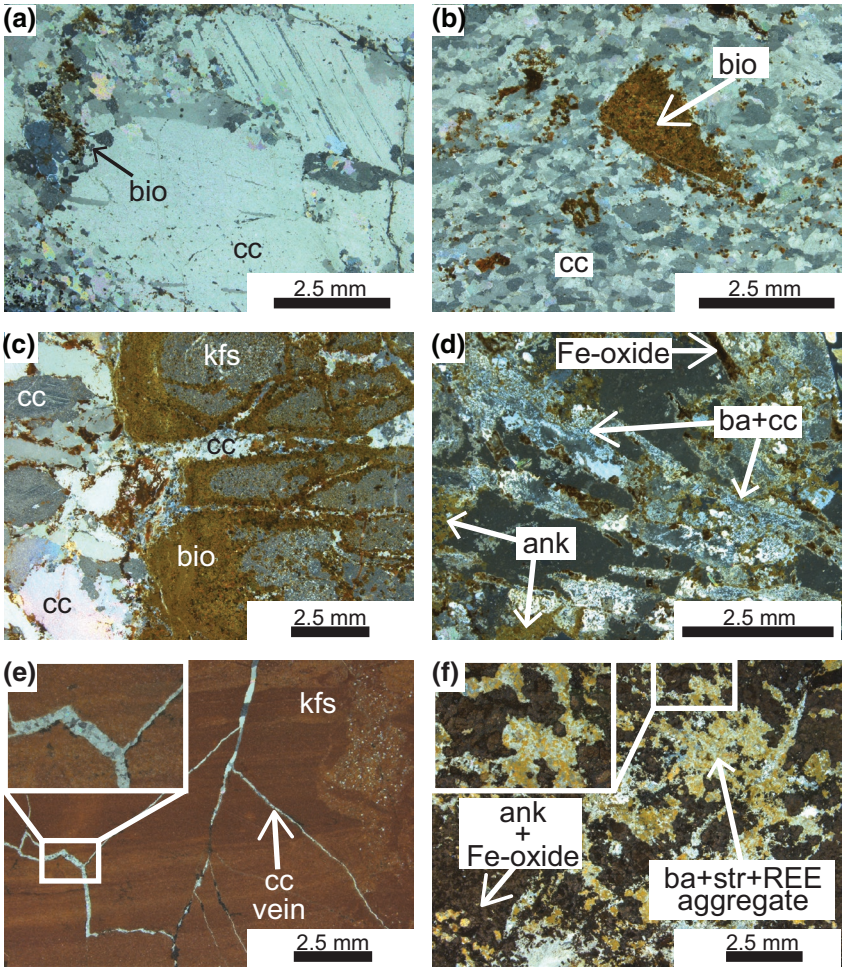

Figure 2. Representative photomicrographs of Khanneshin thin sections under cross-polarized light. (a) Coarse-grained calcite carbonatite (sövite) with fine-grained biotite. Sample RT-10K-9. (b) Medium-grained calcite sövite with a biotite-rich xenolith (i.e., glimmerite). Sample KHAN-1. (c) Larger brecciated fenite xenolith (righthand side) composed of biotite and K-feldspar, hosted in a sövite matrix (left side). Sample KHAN-2. (d) Ankerite-barite carbonatite with lath-shaped intergrowths of barite and calcite. Sample FH-10K-8. (e) Neogene sandstone consisting of K-feldspar and Fe-oxides, crosscut by calcite veins with Mg-Fe-oxide along the rims (black). (f) Ankerite-barite carbonatite with barite-strontianite-REE aggregates that formed by in situ replacement of burbankite (e.g., Anderson et al., 2017). Sample RT-11K-5B6C. Mineral abbreviations: ank, ankerite; ba, barite; bio, biotite; cc, calcium carbonate; kfs, K-feldspar; str, strontianite; REE, rare earth element-rich mineral.

diluted and analyzed on an Agilent 7700 mass spectrometer. Instrumental drift corrections and standardization were done using Ru, In, and Re as internal standards. Long-term precision for REEs is ~5% (1σ).

2.3. Carbon and Oxygen Isotopes

After crushing with an agate mortar and pestle to ~100 um grain size, ~10 mg aliquots of each sample were loaded into 5 mm wide by 5 mm long stainless-steel cups. Sample cups were loaded into a carousel in a double-walled glass vacuum chamber containing an Isocarb common acid bath consisting of 16 ml of 100% phosphoric acid. Under vacuum, each sample was dropped into the acid bath, which was held at 90°C, to degas CO_2. After exposure to acid for 6 min, CO_2 was expanded into a VG Isotech Prism-II stable isotope ratio mass spectrometer for comparative analysis against a calibrated reference gas. One NBS-19 calcite calibration standard of the same approximate mass was analyzed per five unknowns. Typical errors associated with individual Isocarb runs containing pure (>90% $CaCO_3$) carbonate materials are less than ± 0.1‰ for

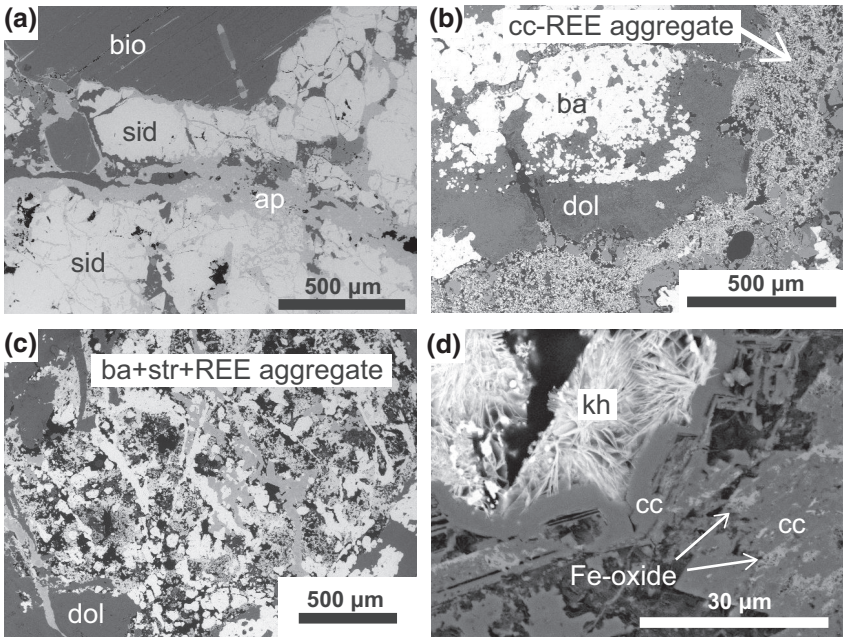

Figure 3. Scanning electron microscope images collected with the secondary electron detector showing Khanneshin mineral textures. (a) An apatite vein in a coarse siderite-biotite matrix. Sample KHAN-3. (b) Barite rimmed by dolomite and calcite-REE mineral aggregate. Sample RT-11K-2B2. (c) Jackson Pollock intergrowth of barite, strontianite, and REE minerals, likely replacing burbankite. Sample RT-11K-2B1. (d) Khanneshite filling a cavity in an intergrowth of calcite and Fe-oxide. Sample RT-10K-03. Mineral abbreviations: ank, ankerite; ba, barite; bio, biotite; cc, calcium carbonate; kfs, K-feldspar; str, strontianite; REE, rare earth element-rich mineral.

$\delta^{13}C$ and ± 0.2‰ for $\delta^{18}O$. Two standard deviations for NBS-19 analyses during Khanneshin sample runs were 0.2‰ for $\delta^{13}C$ and 0.4‰ for $\delta^{18}O$, which was greater than expected. This was likely due to slower dissolution of carbonate phases other than calcite, which continued to release gas during subsequent analyses (i.e., a slight memory effect carrying over into the calibration standards). This contamination would have also affected the unknowns, so we assign uncertainties of 0.2‰ for $\delta^{13}C$ and 0.4‰ for $\delta^{18}O$ for each analysis.

2.4. Thallium Isotopes

Different ~100 mg carbonatite fractions were powdered with an agate mortar and pestle and digested using concentrated HF and HNO_3. Separation of Tl from sample matrix was achieved using a two-stage anion exchange resin (AG1x8) column procedure, the first using 1 ml resin the second using 0.1 ml resin (Nielsen et al., 2004), following the procedure typically used in the NIRVANA lab for rocks (Nielsen et al., 2016). Purified Tl sample solutions were measured in the Woods Hole Oceanographic Institution Plasma Facility using the Neptune MC-ICP-MS (Nielsen et al., 2016). Instrumental mass bias was corrected using Pb (NIST SRM 981) added to the sample solutions, as well as standard-sample bracketing. Thallium isotope compositions are reported relative to the NIST SRM 997 Tl standard in epsilon notation:

$$\varepsilon^{205}Tl = 10{,}000 \times \left[\frac{\frac{^{205}Tl}{^{203}Tl_{sample}} - \frac{^{205}Tl}{^{203}Tl_{SRM\ 997}}}{\frac{^{205}Tl}{^{203}Tl_{SRM\ 997}}} \right]$$

We measured the USGS reference material BHVO-1, which yielded $\varepsilon^{205}Tl = -3.28 \pm 0.15$ (2σ, $n = 4$) in excellent agreement with previous studies (Nielsen, Rehkämper, & Prytulak, 2017). The long-term $\varepsilon^{205}Tl$

Table 1
Major element compositions (wt.%) of khanneshin lavas

Sample	Unit	Latitude	Longitude	SiO_2	Al_2O_3	FeO*	MgO	CaO	Na_2O	K_2O	TiO_2	P_2O_5	MnO	LOI
KHAN-1*	S	30.4738	63.5996	6.48	1.61	4.79	3.57	42.5	0.03	1.91	0.098	1.13	0.69	33.8
KHAN-2*	S	30.4734	63.6011	34.00	8.85	7.30	5.32	16.8	–	8.49	0.196	1.52	0.46	14.1
KHAN-3*	S	30.4732	63.5989	3.44	0.03	74.88	0.99	10.1	–	0.24	0.602	0.96	0.65	6.4
FH-10K-8*	A-B	30.4685	63.5929	–	0.04	1.10	3.75	19.5	0.02	0.10	0.014	0.37	1.14	16.2
FH-10KH-10*	W	30.4738	63.6046	42.24	12.05	5.81	4.40	9.9	0.03	10.40	0.694	0.13	0.28	13.3
RT-10K-03*	A-B	30.4729	63.5979	–	0.66	1.88	1.60	28.6	–	0.66	0.046	0.33	0.84	26.0
RT-10K-5D*	A-B	30.4688	63.5936	–	0.07	12.09	0.69	14.7	–	0.08	0.022	0.42	1.23	17.0
RT-10K-6E*	S	30.4671	63.5922	18.40	4.76	5.18	2.42	16.3	13.08	5.21	0.157	1.02	0.38	31.4
RT-10K-7*	A-B	30.4685	63.5930	–	0.05	1.55	4.75	19.9	–	0.45	0.020	0.18	2.07	15.3
RT-10K-9*	S	30.4708	63.5959	1.66	0.23	4.28	0.75	49.4	0.51	0.45	0.040	2.15	0.61	36.7
RT-10K-11*	A-B	30.4735	63.5982	–	0.37	13.03	2.17	42.3	0.00	0.31	0.074	2.31	1.14	32.1
RT-10K-12*	S	30.4738	63.5996	–	0.40	7.31	0.88	45.6	0.03	0.50	0.073	1.49	5.18	32.5
RT-11K-1	A-B	30.4797	63.5949	0.99	0.07	1.84	5.25	23.0	0.08	0.17	0.001	0.25	1.16	21.2
RT-11K-2B1	A-B	30.4792	63.5954	0.22	0.03	3.14	6.31	16.9	0.23	0.02	0.01	1.76	1.78	23.2
RT-11K-2B2	A-B	30.4792	63.5954	0.2	0.02	2.98	6.07	17.2	0.26	0.02	–	2.03	1.82	22.7
RT-11K-4A0	A-B	30.4784	63.5945	0.35	0.06	0.75	5.63	36.2	0.48	3.13	–	0.07	0.48	35.0
RT-11K-5A1	A-B	30.4782	63.5945	0.35	0.06	2.51	6.85	16.9	0.12	0.13	–	0.20	1.97	18.0
RT-11K-5B1A	A-B	30.4782	63.5945	0.39	0.05	2.79	6.63	16.1	0.19	0.13	–	1.29	2.28	18.5
RT-11K-5B3B	A-B	30.4782	63.5945	0.34	0.05	1.81	4.94	20.1	0.13	0.08	–	0.54	1.80	16.3
RT-11K-5B4*	A-B	30.4782	63.5945	–	0.04	1.62	4.66	13.6	–	0.11	0.017	1.09	1.90	16.3
RT-11K-5B6C	A-B	30.4782	63.5945	1.18	0.21	8.14	10.01	20.9	0.1	0.25	0.01	0.09	3.91	27.8
RT-11K-6	A-B	30.4781	63.5945	2.11	0.49	6.48	6.86	19.2	3.87	0.64	0.02	1.08	2.58	30.2

Note. Total Fe is expressed as FeO*. All samples denoted with an asterisk were not previously reported in Tucker et al. (2011). LOI stands for loss on ignition. Abundances below detection limits are marked by hyphens.
A-B, ankerite-barite carbonatite; S, sövite; W, wall rock sandstone.

reproducibility (2σ) for both USGS reference materials (sediments and igneous rocks) as well as seawater is 0.3–0.4 epsilon units with these methods (Nielsen et al., 2015; Ostrander et al., 2017; Owens et al., 2017), which is due to the exceptional affinity of Tl for anion exchange resins (Nielsen et al., 2017). Because Khanneshin samples contain higher concentrations of Tl and thereby produce analyses with ion beam intensities in excess of the references standards, we consider 0.3 epsilon units to be a conservative estimate for the uncertainty associated with each analysis, except for two samples (RT-10K-03 and RT-10K-5D) where repeat analyses on the same solution were not reproducible to within 0.3 epsilon units.

3. Results

3.1. Whole-Rock Geochemistry

Due to the abundance of volatile elements in Khanneshin samples, large mass fractions (6–37 wt%) were lost on ignition (LOI) during XRF analyses (Table 1). LOI correlates positively with CaO, indicating that carbonate-derived CO_2 from calcite dominated the lost mass. Note, however, that Sr and Ba account for multiple wt% in some samples (Tucker et al., 2011) and are not used for the LOI calculation. With the exception of CaO, all elements measured by XRF vary by 1–2 orders of magnitude in Khanneshin samples. SiO_2 ranges from below detection (~0.1 wt%) to 42 wt% and Al_2O_3 ranges from 0.02 to 12 wt%. Notably, only samples with high mica contents (KHAN-1, KHAN-2, RT-10K-6E) and the sandstone (FH-10KH-10) have SiO_2 and Al_2O_3 greater than several wt%. Total iron (FeO*) is also highly variable, ranging from 1 wt% to 75

Table 2
Rare earth element concentrations for khanneshin lavas reported in μg/g

Sample	La	Ce	Pr	Nd	Sm	Eu	Gd	Tb	Dy	Ho	Er	Tm	Yb	Lu
KHAN-1*	259	614	66	280	96	28	100	15.1	70	10.8	22.2	2.5	12.1	1.6
KHAN-2*	722	1025	89	296	52	12	39	6.1	33	5.6	12.0	1.3	6.6	0.9
KHAN-3*	220	412	36	120	18	4	12	1.5	7	1.1	2.4	0.3	1.5	0.2
FH-10K-8	7530	11254	849	2157	190	72	214	10.2	15	1.7	10.4	0.5	3.8	0.6
FH-10KH-10	31	62	7	29	10	4	15	3.0	21	4.0	10.8	1.5	9.5	1.4
RT-10K-3	9198	10536	674	1430	119	50	198	10.5	25	3.6	12.7	1.0	5.0	0.7
RT-10K-5D	6562	11053	862	2285	207	71	227	11.0	18	2.0	10.7	0.4	2.5	0.3
RT-10K-6E	65	142	17	70	12	3	10	1.0	5	0.7	1.8	0.2	1.2	0.2
RT-10K-7	7838	7101	441	1048	83	7	113	5.1	13	1.7	6.7	0.6	4.4	0.6
RT-10K-9	426	919	108	430	68	17	65	8.3	43	6.6	16.1	1.8	10.1	1.3
RT-10K-11	1484	3215	355	1396	209	53	178	17.0	65	8.2	19.5	1.8	10.1	1.3
RT-10K-12	458	986	117	473	88	25	96	14.0	74	10.8	24.4	2.7	14.2	2.0
RT-11K-1	10300	14600	1110	2880	258	40	109	6.9	26	3.4	8.3	1.0	5.8	0.9
RT-11K-2B1	8620	11700	1010	3090	415	85	271	36.5	162	20.8	40.4	3.8	17.1	2.1
RT-11K-2B2	7980	11200	992	3060	417	85	267	36.2	160	20.9	39.8	3.8	16.9	2.1
RT-11K-4A0	5550	7940	720	2160	231	38	92	6.1	23	3.1	8.6	1.2	8.4	1.3
RT-11K-5A1	5990	13000	1240	3690	507	110	349	44.1	181	19.9	32.8	2.8	12.6	1.6
RT-11K-5B1A	5380	11900	1180	3600	508	109	352	46.2	201	23.8	42.3	3.7	15.8	1.8
RT-11K-5B3B	6400	13300	1270	3990	626	136	431	55.5	236	25.5	38.2	3.0	12.7	1.5
RT-11K-5B4*	5773	13086	1407	4387	564	127	402	56.3	234	28.1	41.6	3.6	14.6	1.6
RT-11K-5B6C	21000	31500	2600	7090	657	102	274	15.8	47	5.0	11.0	1.4	8.3	1.4
RT-11K-6	16600	23000	1980	5800	615	102	279	22.5	91	11.4	22.0	2.2	9.7	1.1

Note. All samples except those denoted with an asterisk are reported in Tucker et al. (2011).

wt% (KHAN-3). All of the samples have <0.5 wt% Na_2O, except RT-10K-6E (13 wt%) and RT-11K-6 (4 wt%). Sample KHAN-2 is anomalous with respect to K_2O, containing nearly as much K_2O (9 wt%) as the K-feldspar sandstone, sample FH-10KH-10 (10 wt%). These two samples also contain the highest TiO_2 (~0.6 wt%). MnO ranges from 0.3 to 5.2 wt% and values above 1 wt% are only measured in samples with K_2O < 1 wt% (and vice versa). P_2O_5 ranges from 0.07 wt% (RT-11K-4AO) to 2.3 wt% (RT-11K-11) in ankerite-barite carbonatite samples and does not correlate with other major element abundances.

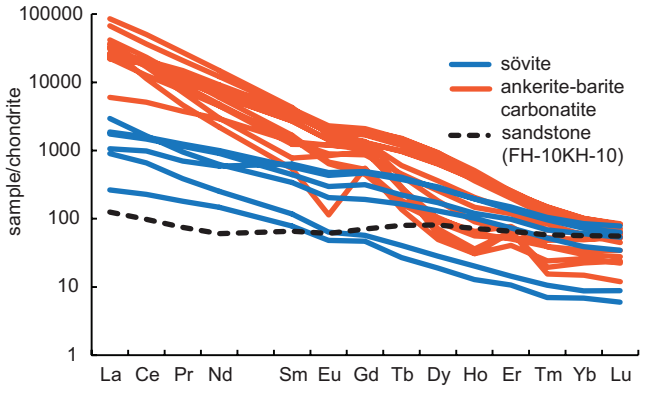

Figure 4. Rare earth element concentrations for Khanneshin carbonatite samples normalized to chondrite (O'Neill, 2016). The ankerite-barite carbonatites have higher LREE contents than the sövites.

REE concentrations in the carbonatites (Table 2) are up to five orders of magnitude greater than chondrite (Figure 4). Total light REE (LREE: La through Eu) contents in the carbonatite samples range from 300 μg/g in sövite (RT-10K-6E) to 6 wt% in late-stage veins in ankerite-barite carbonatite (RT-11K-5B6C). In comparison, total heavy REE (HREE: Gd through Lu) contents are relatively modest, ranging from 19 μg/g in sövite (RT-10K-6E) to 800 μg/g in late-stage veins (RT-11K-5B3B). La concentrations correlate positively with La/Yb (Figure 5a), indicating that high LREE contents do not correspond to proportionally high HREE contents. With the exception of one sample (RT-10K-7), negative Eu anomalies are absent. Several samples (RT-10K-7, RT-10K-8, and RT-10K-5D) reported by Tucker et al. (2011) have positive Er anomalies that are probably artifacts of isobaric interferences with oxides; this is not observed in the new

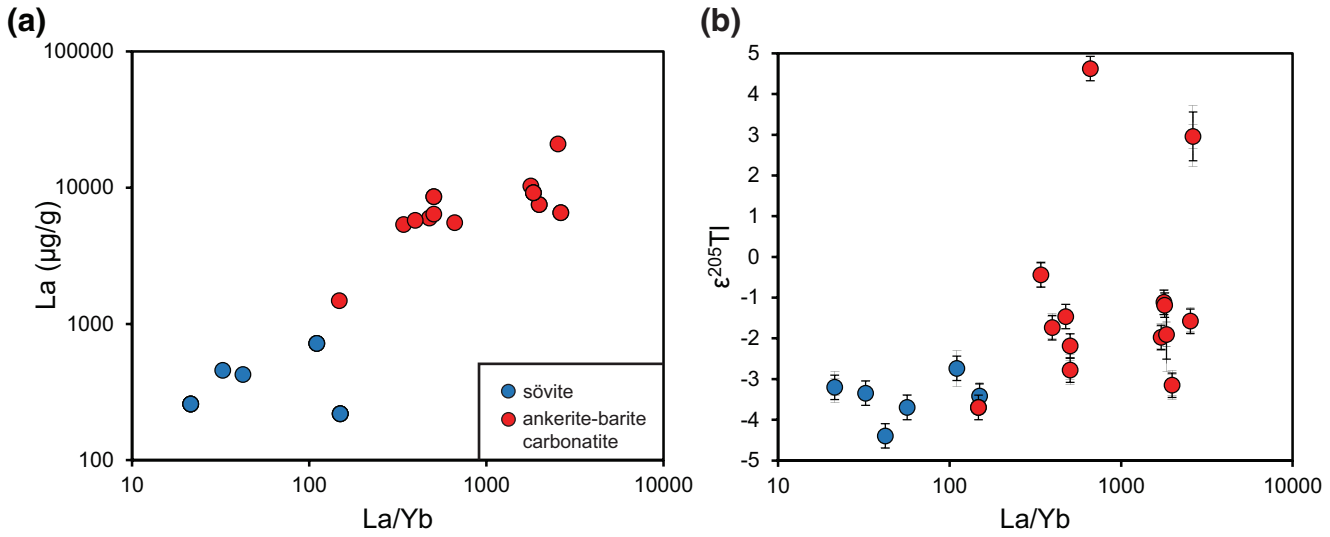

Figure 5. (a) La concentration in Khanneshin samples correlates with La/Yb ratios. (b) Only samples with La/Yb greater than 200 have ε^{205}Tl values greater than −2. Mean values are plotted for samples with repeated Tl analyses.

ICPMS data. Previous studies did not analyze Cs, but we measured Cs concentrations in samples KHAN-1 (4.90 µg/g), KHAN-2 (9.04 µg/g), KHAN-3 (0.56 µg/g), and RT-11K-5B4 (0.03 µg/g) by ICPMS.

3.2. Carbon and Oxygen Isotopes

Khanneshin samples have $\delta^{13}C_{VPDB}$ from −4.6‰ to +3.5‰ and $\delta^{18}O_{VSMOW}$ from +8.6‰ to +23.5‰. $\delta^{13}C$ and $\delta^{18}O$ are positively correlated (Table 3, Figure 6a), except for the highest $\delta^{18}O$ (>20‰) samples; the slope of this trend decreases from ~0.8 for data with $\delta^{18}O$ < 15‰ to ~0.5 at $\delta^{18}O$ 15‰–20‰. Overall, sövites have lighter isotopic compositions than ankerite-barite carbonatites. Sövite sample RT-10K-9 ($\delta^{13}C$ = −4.6‰) is the only Khanneshin rock with $\delta^{13}C$ less than −2.5‰, above which there is a nearly continuous spread of $\delta^{13}C$ compositions. Two anomalous ankerite-barite carbonatites (RT-11K-5A1 and RT-11K-5B4) have relatively low $\delta^{13}C$ (~0‰) and relatively high $\delta^{18}O$ (>14‰). The sandstone (FH-10KH-10) has $\delta^{13}C$ and $\delta^{18}O$ comparable to the isotopically heaviest carbonatites.

Repeat analyses indicate that there is intrasample isotopic variability that exceeds analytical uncertainty. For example, repeat analyses of KHAN-1, KHAN-2, and KHAN-3 have $\delta^{13}C$ and $\delta^{18}O$ that vary by 0.8–1.8 ‰ and 1.3–1.7 ‰, respectively. A repeat analysis of RT-10K-5D yielded much heavier isotopic ratios (3.3‰ and 4.4‰ heavier for $\delta^{13}C$ and $\delta^{18}O$, respectively) than the first result. In nearly all cases, repeat analyses exhibited corresponding changes in both isotopic systems, suggesting that intrasample isotopic variability is similar to—but lesser in magnitude than—the carbon-oxygen isotopic trend defined by the full data set.

3.3. Thallium Isotopes

The Tl abundance in Khanneshin samples varies by two orders of magnitude from ~250 ng/g to >30 µg/g (Table 4) and does not correlate with REE content. Thallium isotope compositions range from ε^{205}Tl = −4.6 ± 0.3 (RT-10K-9) to +4.6 ± 0.3 (RT-11K-4AO) and are not correlated with Tl concentration. Notably, only ankerite-barite carbonatites with La/Yb greater than 200 have ε^{205}Tl higher than −2 (Figure 5b). Only two of these (RT-10K-5D and RT-11K-4AO) yielded ε^{205}Tl greater than zero.

Table 3
Carbon and oxygen isotopic compositions of khanneshin samples, expressed in the delta notation (‰)

Sample	$\delta^{13}C_{VPDB}$	$\delta^{18}O_{VSMOW}$
FH-10K-8	3.17	22.5
	3.24	22.3
FH-10KH-10	3.29	20.9
KHAN-1	−1.12	11.6
	−1.51	10.5
	−1.89	9.9
	−1.92	11.0
KHAN-2	−1.96	11.0
	−0.48	12.0
	−0.19	12.3
KHAN-3	−2.18	10.0
	−1.67	10.2
	−1.46	10.4
	−0.82	11.3
RT-10K-03	1.13	13.8
RT-10K-11	−1.86	9.4
RT-10K-12	0.41	12.0
RT-10K-5D	0.95	16.1
	−2.31	11.8
RT-10K-9	−4.61	8.6
RT-10K-3	0.68	12.9
	0.75	12.8
RT-11K-1	3.48	18.2
RT-11K-2B1	2.02	23.5
RT-11K-2B2	2.45	19.1
RT-11K-4A0	2.38	17.8
RT-11K-5A1	−0.36	13.6
RT-11K-5B1A	2.71	19.5
RT-11K-5B3B	3.22	19.7
RT-11K-5B4	0.32	11.8
RT-11K-5B6C	2.43	22.7

Note. Note that there are repeat analyses of some samples. 2σ uncertainties for δ13C and δ18O are 0.2‰ and 0.4‰, respectively.

4. Discussion

The positive correlation between $\delta^{13}C$ and $\delta^{18}O$ at $\delta^{18}O$ +5‰ to +15‰ is too strong and too consistent among carbonatite complexes worldwide to be coincidental and, therefore, must reflect a fundamental carbonatite process (Deines, 1989). Below, we use this $\delta^{13}C$-$\delta^{18}O$ correlation in Khanneshin rocks to construct fractionation models that provide context for interpreting our Tl isotopic results. In a complementary manner, insights gained from our Tl isotopic results provide an improved framework for interpreting $\delta^{13}C$ and $\delta^{18}O$ variability in carbonatites.

4.1. Carbon and Oxygen Isotopic Variability

In $\delta^{13}C$ vs. $\delta^{18}O$ space (Figure 6a), Khanneshin samples are outside the range of primary igneous carbonatites, as first defined by Taylor et al. (1967): $\delta^{13}C$ from −8.0‰ to −5.0‰ and $\delta^{18}O$‰ from +6.0‰ to +8.5‰. Although several samples with $\delta^{18}O > 15$ ‰ fall within the limestone range defined by Bell and Simonetti (2010), two sövite samples (RT-10K-9 and KHAN-1)—presumably the least geochemically evolved—plot near the canonical mantle range. The lower REE contents of the sövites and the existence of sövite xenoliths in the ankerite-barite carbonatites confirm that sövites represent the least evolved magma compositions. Degassing of CO_2 cannot explain the $\delta^{13}C$ and $\delta^{18}O$ trends because (a) the residual carbonatite fluids would become isotopically lighter and (b) CO_2 degassing would have a lesser effect on $\delta^{18}O$ due to the abundance of O in the system. Mica-rich xenoliths testify to magmatic assimilation of metasomatized wall rock, but this is not a viable explanation for $\delta^{13}C$ and $\delta^{18}O$ variability for two reasons. First, assimilation of silica-rich wall rock material would not have contributed much carbon to the system and cannot explain extent of $\delta^{13}C$ variability. Second, sample KHAN-2 has the highest Si content and contains the greatest fenite xenolith component based on petrographic observations; the intermediate $\delta^{18}O$ of this sample implies that xenoliths are not a reasonable $\delta^{18}O$ endmember. Note also that, unlike at Ol Doinyo Lengai, where trace element and Sr-Nd-Pb isotopic compositions covary due to wall rock assimilation (Kramm & Sindern, 1998), Khanneshin lavas have nearly homogenous Sr-Nd-Pb isotopic compositions (Ayuso et al., 2013) that are inconsistent with large amounts of crustal assimilation.

Carbonatite complexes worldwide exhibit similar $\delta^{13}C$ and $\delta^{18}O$ ranges (e.g., Deines & Gold, 1973), which are generally attributed to some combination of calcite crystallization, hydrothermal activity, and weathering (Keller & Hoefs, 1995; Pineau et al., 1973; Taylor et al., 1967). Isotopic fractionation by one or more of these processes can explain a temporal isotopic progression in Khanneshin rocks from near-mantle values in sövites to heavier $\delta^{13}C$ and $\delta^{18}O$ compositions in ankerite-barite carbonatites. This is also consistent with the observation that the sandstone (FH-10KH-10) has one of the highest (i.e., most evolved) $\delta^{13}C$ values because vein calcite is the dominant host of C in the sample and likely precipitated from late-stage fluids. Intrasample variability (up to several per mil) suggests that individual samples record multiple stages of isotopic evolution, which is also evidenced by mineral textures that vary on the thin section scale in most of the samples.

4.2. Rayleigh Fractionation Models

As discussed above, wall rock assimilation can be ruled out as the primary cause of $\delta^{13}C$ and $\delta^{18}O$ variations on the basis that the silica-rich wall rock has an inferred moderate $\delta^{18}O$ composition. Nor are magmatic

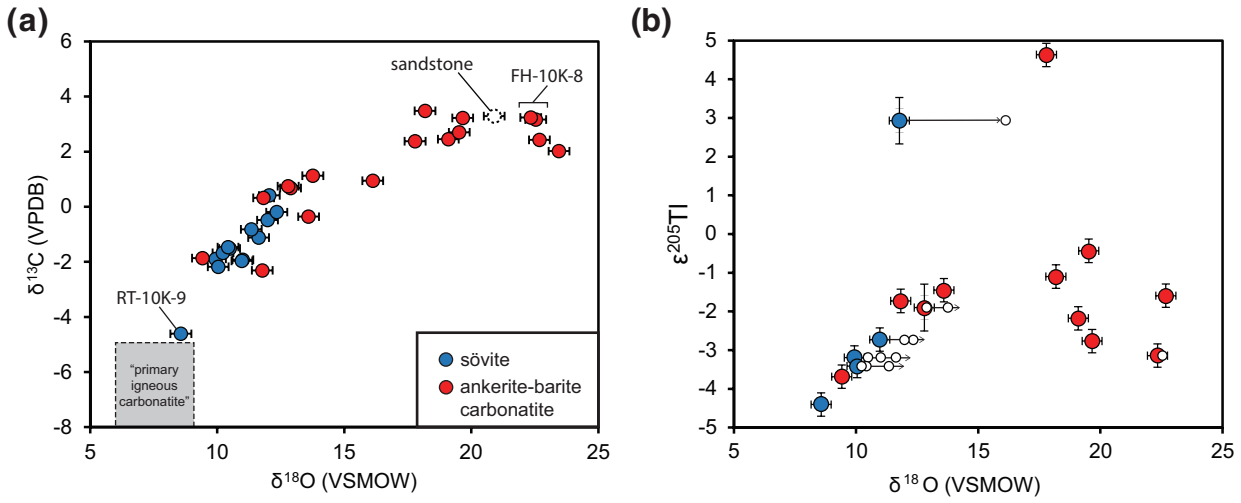

Figure 6. (a) Carbon and oxygen isotopic compositions for Khanneshin volcano samples (including reruns). All samples are isotopically heavier than primary igneous carbonatites, as defined by Taylor et al. (1967). Ankerite-barite carbonatites generally have lighter isotopic compositions. (b) Thallium isotopic results—from different powdered portions of the same samples—also correlate positively with $\delta^{18}O$ for those samples with $\delta^{18}O < 15‰$. We assume that the lowest $\delta^{18}O$ value measured for each sample represents the least evolved composition (colored symbols). Repeat $\delta^{18}O$ measurements are plotted as small white circles to show the isotopic variability within each sample; small black arrows indicate the isotopic trend away from the least evolved compositions. Error bars represent 2σ uncertainties.

processes a likely cause for large $\delta^{13}C$ and $\delta^{18}O$ variations: Isotopic fractionation during fractional crystallization, or between silicate and carbonatitic melts, typically affect the $\delta^{13}C$ and $\delta^{18}O$ of magmas by less than ~2‰ (Santos, 1995). Instead, large variations can be explained by isotopic fractionation between carbonate minerals and a CO_2- and H_2O-rich fluid (Pineau et al., 1973; Ray & Ramesh, 2000; Santos, 1995).

We use a Rayleigh fractionation model (after Pineau et al., 1973) to evaluate the isotopic evolution of a CO_2-H_2O fluid as it is consumed by the precipitation of calcite:

$$CO_2 + H_2O + Ca^{2+} \rightleftharpoons CaCO_3 + 2H^+.$$

The $\delta^{13}C$ composition of a CO_2-H_2O fluid can be described by:

$$\delta^{13}C_{\text{fluid}} - \delta^{13}C_0 \cong 1000\left(\alpha^{13}C_{\text{cal}-CO_2} - 1\right) \times \ln\left(f_C\right).$$

where $\delta^{13}C_0$ is the initial fluid composition, $\alpha^{13}C$cal-CO_2 is the fractionation factor between calcite and CO_2, and f_C is the fraction of the initial carbon remaining in the fluid. The $\delta^{18}O$ composition is affected by calcite-CO_2 *and* calcite-H_2O fractionation; it therefore also depends on the initial molar H_2O:CO_2 in the fluid (yH_2O-CO_2). We use the model provided by Pineau et al. (1973), described at length by Ray and Ramesh (2000):

$$\delta^{18}O_{\text{fluid}} - \delta^{18}O_0 \cong 1000\left[\left(\alpha^{18}O_{\text{cal-}CO_2} - 1\right) - \frac{1}{3}\left(\alpha^{18}O_{H_2O-CO_2} - 1\right)\right] \times \ln\left(f_O\right) + 1000\left[\frac{2}{3}\left(\frac{1 - y_{H_2O-CO_2}}{2 + y_{H_2O-CO_2}}\right)\left(\alpha^{18}O_{H_2O-CO_2} - 1\right)\left(1 - \frac{1}{f_O}\right)\right],$$

where $\delta^{18}O_0$ is the initial fluid composition, $\alpha^{18}O$cal-CO_2 is the fractionation factor between calcite and CO_2, $\alpha^{18}OH_2O$-CO_2 is the fractionation factor between H_2O and CO_2, and f_O is the fraction of the initial oxygen remaining in the fluid. Carbonatites elsewhere crystallize at 550–700°C (Haynes et al., 2003), so we assume isothermal conditions at 700°C and obtain $\alpha^{13}C$cal-CO_2 (0.99652) and $\alpha^{18}O$cal-CO_2 (0.99509) using

Table 4
Thallium isotopic compositions of khanneshin samples, expressed in the epsilon notation

Sample	ε^{205}Tl	Tl (ng/g)
FH-10K-8	−3.19	708
	−3.1	717
KHAN-1	−3.11	30329
	−3.28	30471
KHAN-2	−2.59	2780
	−2.87	2802
KHAN-3	−3.44	4508
	−3.38	4529
RT-10K-03	−1.29	6635
	−2.51	6708
RT-10K-5D	3.42	25057
	2.51	25198
RT-10K-6E	−3.69	1246
RT-10K-7	−1.18	608
RT-10K-9	−4.39	2358
RT-10K-11	−3.69	9264
RT-10K-12	−3.34	15025
RT-11K-1	−1.11	5123
RT-11K-2B2	−2.18	249
RT-11K-4A0	4.63	299
RT-11K-5A1	−1.46	3722
RT-11K-5B1A	−0.42	948
	−0.45	
RT-11K-5B3B	−2.71	311
	−2.84	317
RT-11K-5B4	−1.7	446
	−1.76	455
RT-11K-5B6C	−1.54	1925
	−1.6	1955
RT-11K-6	−2	703
	−1.94	717

Note. Note that there are repeat analyses of some samples. 2σ uncertainties for each sample are 0.3 ε^{205}Tl-units, except for RT-10K-03 and RT-10K-5D, which have uncertainties of ∼0.6 ε^{205}Tl-units.

a second-order polynomial fit to the results of Scheele and Hoefs (1992). For $\alpha^{18}OH_2O\text{-}CO_2$, we use 0.99665, which is the ratio of the β factors for oxygen exchange between H_2O (1.0163) and CO_2 (1.0129) at 700°C from Richet et al. (1977). These fractionation factors decrease with increasing temperature above 500°C, but this has a relatively minor effect on the magnitude of fractionation in the models. For example, at 800°C rather than at 700°C, the model predicts calcite $\delta^{18}O$ and $\delta^{13}C$ that are less extreme by at most 0.6‰ and 0.3‰, respectively.

Because f_C and f_O diverge if $y H_2O\text{-}CO_2 \neq 1$, we calculate f_O as a function of f_C (after Ray & Ramesh, 2000, Equation 11):

$$f_O = \frac{3f_C - \left(1 - y_{H_2O-CO_2}\right)}{\left(2 + y_{H_2O-CO_2}\right)}$$

The model predicts that the CO_2-H_2O fluid and the calcite in equilibrium with it become isotopically heavier with respect to both $\delta^{13}C$ and $\delta^{18}O$ as the fluid is consumed by calcite precipitation. When $y H_2O\text{-}CO_2 = 1$, the isotopic evolution is linear. However, when $y H_2O\text{-}CO_2 > 1$, oxygen is preferentially consumed. In this case, as f_O approaches zero, $\delta^{18}O$ fractionation outpaces that of $\delta^{13}C$.

The above model can produce $\delta^{13}C$ and $\delta^{18}O$ trends similar to those observed in Khanneshin rocks. Various initial $\delta^{13}C$ and $\delta^{18}O$ compositions lighter than −5‰ and +8‰, respectively, yield curves that fit Khanneshin data reasonably well, so the model does not shed light on the primary isotopic composition of the magmas beyond the fact that they must have been lighter than the lightest recorded value ($\delta^{13}C = -4.5$‰ and $\delta^{18}O = +9$‰). Nevertheless, the model results are consistent with mantle-like initial values ($\delta^{13}C = -6$‰ and $\delta^{18}O = +5$‰: Deines & Gold, 1973; Taylor et al., 1967). Calcite precipitating from a fluid with $y H_2O\text{-}CO_2 = 1$ can explain the linear $\delta^{13}C$-$\delta^{18}O$ trend when $\delta^{18}O < 15$‰ (Figure 7a). If $y H_2O\text{-}CO_2$ is ∼0.9, $\delta^{18}O$ fractionation outpaces $\delta^{13}C$ fractionation, which provides a better fit to the full data set (Figure 7b). This indicates that the highest $\delta^{18}O$ values may have resulted from calcite precipitation from a residual fluid with high CO_2/H_2O in which only 2%–7% of the initial O remained (Figure 7b). Complex open-system behavior may have influenced the CO_2/H_2O ratio in numerous ways. Decarbonation reactions may have increased CO_2/H_2O by adding CO_2 to the fluids and, in the case of biotite fenitization, consuming H_2O. Exsolution of both species from other fluids (magma or brine) would also alter the CO_2/H_2O ratio. Alternatively, a CO_2-H_2O fluid with equal molar proportions may have been consumed (or perhaps escaped) by the time the Khanneshin carbonatite system evolved to $\delta^{18}O$ ∼15‰, after which $\delta^{18}O$ fractionation was driven by interactions with meteoric fluids (Figure 7a). In all cases, a significant CO_2 component is necessary to explain the spread of $\delta^{13}C$ in Khanneshin lavas.

4.3. Thallium Isotope Systematics

Average Khanneshin carbonatite ε^{205}Tl values are generally similar to average continental crust and the depleted MORB mantle (Figure 8a; Nielsen et al., 2017), although the total range in Khanneshin rocks exceeds the relatively invariant values found in these reservoirs. Tl concentrations range from near continental crust levels (300–500 ng/g; Hans Wedepohl, 1995) to those of ferromanganese marine sediments (∼10–200 μg/g; Nielsen et al., 2013), which are highly enriched compared to the other geochemical reservoirs. Three of

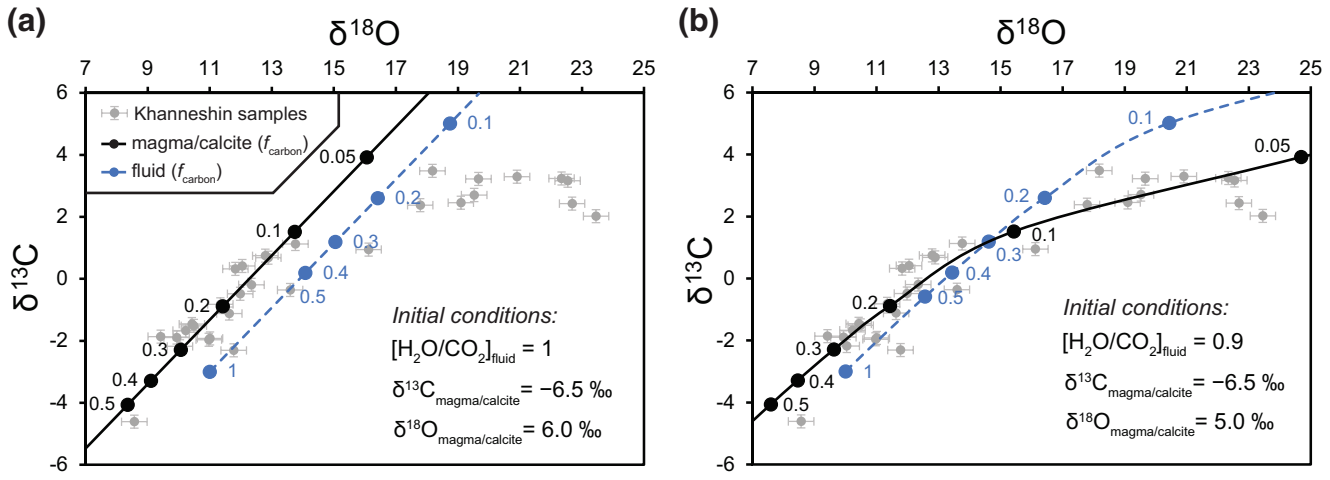

Figure 7. Rayleigh fractionation models that describe the isotopic evolution of calcite in equilibrium with an H_2O-CO_2 fluid that is consumed by calcite formation at 700°C. (a) When the initial H_2O/CO_2 ratio of the fluid equals one, $\delta^{18}O$ fractionation is proportional to $\delta^{13}C$ fractionation. (b) When the initial H_2O/CO_2 ratio is less than one, $\delta^{18}O$ fractionation outpaces $\delta^{13}C$ fractionation as the oxygen reservoir becomes depleted. Depending on initial magma isotopic compositions, either model can explain the trend observed in Khanneshin samples (shown in gray for reference, with 2σ uncertainties) with $\delta^{18}O < 15‰$. A model with initial H_2O/CO_2 ratio of 0.9 produces a better fit for the entire Khanneshin data set. The numbers next to black (calcite) and blue (fluid) symbols show the fraction of carbon remaining in the fluid (f_c).

the four samples in which we measured Cs—a geochemical tracer of slab-derived fluids in magmatic arcs (Spandler & Pirard, 2013)—have Cs/Tl less than depleted MORB mantle and subducting sediments (Figure 8b). Thus, the high Tl concentrations and low Cs/Tl ratios in Khanneshin rocks distinguish them from most igneous and sedimentary rocks. The measured Cs/Tl ratios, however, may not represent the compositions of primary Khanneshin magmas.

As for carbon and oxygen isotopes, wall rock assimilation is not a reasonable explanation for Tl isotopic variability in Khanneshin rocks. Xenolith-rich sample KHAN-2 might best represent assimilated wall rock and has an intermediate Tl concentration (2.8 μg/g) and isotopic composition ($\varepsilon^{205}Tl = -2.7$) with respect to other data in this study. This is not a viable endmember composition.

$\varepsilon^{205}Tl$ and REE systematics are coupled in Khanneshin carbonatites. REE incompatibility in solid phases during igneous differentiation can explain why REEs became concentrated in evolved Khanneshin magmas (e.g., Anenburg et al., 2020). As in carbonatite complexes elsewhere (e.g., Thompson et al., 2002;

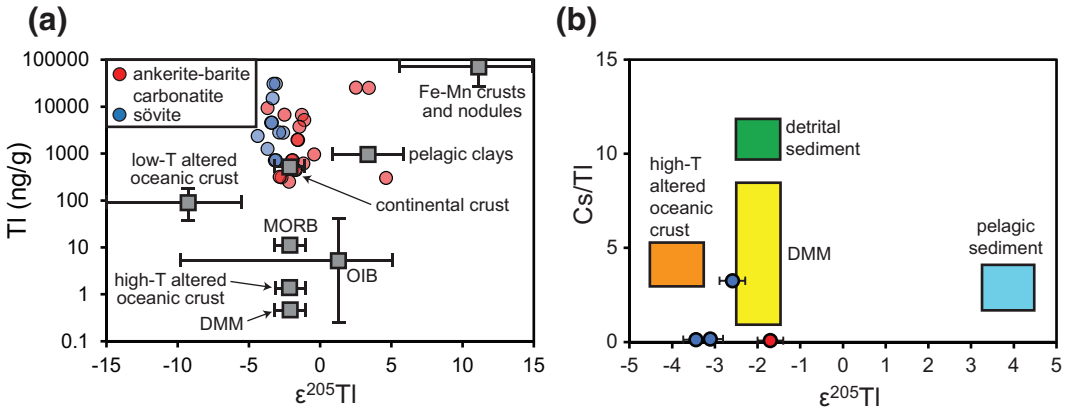

Figure 8. Thallium isotopic results for Khanneshin carbonatite samples. (a) Thallium concentrations and isotopic compositions exceed average MORB, ocean island basalt (OIB), depleted MORB mantle (DMM), and high-T altered oceanic crust (after Nielsen et al., 2017). Two-sigma $\varepsilon^{205}Tl$ uncertainties are approximately the width of the symbols. (b) Cs data exist for four Khanneshin carbonatite samples and Cs/Tl ratios for three of these samples are well below well characterized geochemical reservoirs (after Nielsen et al., 2016).

Woolley, 1982), REE enrichment coincided with Fe and Mg enrichment in residual ankerite-barite magmas compared to the less evolved sövites. Light and heavy REEs are strongly incompatible in calcite, dolomite, and ankerite. The incorporation of REE^{3+} ions in Ca^{2+} sites requires charge balance by other cations (e.g., Na^{+}) and the resulting coupled substitutions exert strain on the crystal lattice (Chakhmouradian et al., 2016). For this reason, the fractional crystallization of calcite can explain elevated REE and Tl concentrations in residual magmas and fluids, but not the elevated La/Yb ratios. Instead, the observed increase of La/Yb is probably due to the fact that HREEs are preferentially delivered to the wall rock during metasomatism by alkali-rich brines (Anenburg et al., 2020). Such fluids are commonly associated with carbonatite magmatism, but whether they are end products of fractional crystallization (Anenburg et al., 2020), liquid immiscibility (Newton & Manning, 2002, 2010), or both remains controversial. In any case, REEs complex with alkali elements in carbonatite-derived brines until interactions with wall rock in fenite zones consume the alkalis, causing REE precipitation in alkali-free phases (Anenburg et al., 2020).

The fact that samples with ε^{205}Tl greater than −2 exclusively have La/Yb ratios higher than 200 (Figure 5b) suggests that Tl isotopic fractionation to heavier compositions coincided with La/Yb increases and, thus, alkali-rich hydrous brine activity. Tl behavior in carbonatitic systems is not well understood. Biotite may preferentially retain ^{203}Tl in igneous and metamorphic silicic systems (Rader et al., 2018), so it seems reasonable that biotite crystallization during fenitization would also increase the ε^{205}Tl in residual carbonatitic systems. Too little primary igneous biotite occurs in Khanneshin lavas to explain this trend. Therefore, we propose that La/Yb and ε^{205}Tl increases are driven by metasomatism of wall rock by alkali-rich brines. Fenite xenolith-bearing samples (e.g., KHAN-2) do not have higher Tl and HREE concentrations than other samples, suggesting that these components may not strongly partition into fenite. On the other hand, the xenolith-bearing samples may not be representative of subsurface fenite zones.

ε^{205}Tl correlates positively with δ^{18}O in Khanneshin carbonatites with $\delta^{18}O < 15‰$ (Figure 6b); this trend has a slope of ∼0.6. Because we used different sample powders for carbon-oxygen isotopes, Tl analyses, and major element oxide plus REE analyses, intrasample variability is probably responsible for some scatter when comparing results from different techniques. Here, we assume that the lowest δ^{18}O (nearest to presumed mantle values) is the least evolved composition and best represents the bulk carbonatite that hosts the Tl (colored symbols in Figure 6b). Heavier δ^{18}O values for the same samples (white circles in Figure 6b) probably reflect equilibration with fluids that underwent more Rayleigh fractionation or mixed with material in late-stage veins. Regardless of these variations, however, the positive correlation between ε^{205}Tl and δ^{18}O below δ^{18}O of 15‰ is robust. High ε^{205}Tl and high δ^{18}O analyses that deviate from this trend might reflect partial resetting of the Tl isotopic system by meteoric fluids—resulting in high ε^{205}Tl—or the cessation of biotite growth, which would have arrested Tl isotopic evolution. Degassing may fractionate Tl isotopes (e.g., Baker et al., 2009), but the covariation with carbon and oxygen isotopes indicates that degassing was not the primary cause of Tl isotope variations. Rather, calcite precipitation in equilibrium with a CO_2-H_2O-rich fluid and metasomatism that caused Tl isotopic fractionation were concurrent.

In summary, Khanneshin lavas exhibit systematic increases in (i) total REEs, (ii) La/Yb, (iii) ε^{205}Tl, (iv) δ^{13}C, and (v) δ^{18}O from early (sövite) to late-stage (ankerite-barite) carbonatites. These results imply simultaneous (i) igneous differentiation, (ii) hydrous brine activity, (iii) biotite metasomatism, and (iv and v) isotopic fractionation between CO_2 and carbonatite minerals, respectively. This precludes scenarios in which igneous differentiation subsided prior to metasomatism and highlights the active role of CO_2 in carbonatitic systems.

4.4. Implications for Carbonatite Genesis

Primary carbonatitic magmas may form when parental carbonated silicate magmas differentiate into immiscible carbonatitic and alkaline silicate magmas. At Khanneshin volcano, no voluminous silicate alkaline magmas reached the surface. The volcanic plugs of phonolite are too small to be a complimentary silicate magmatic system, although we cannot rule out the existence of larger subsurface phonolite bodies. Khanneshin carbonatites have alkali element (K and Na) concentrations too low to be in equilibrium with immiscible alkaline silicate magmas (e.g., Hamilton et al., 1979), which is a common geochemical feature of carbonatite complexes worldwide (Ol Doinyo Lengai is a notable exception). Loss of K and Na during meta-

somatism of wall rock (also referred to as fenitization) causes lower-than-expected abundances of these elements in carbonatites (Anenburg et al., 2020; Rubie & Gunter, 1983; Weidendorfer et al., 2016). The copious mica-rich xenoliths in Khanneshin sövite samples attest to metasomatism (e.g., Giebel et al., 2019) that began prior to eruption. Sustained fenitization-related alkali element loss during eruption is consistent with Tl isotopic trends in Khanneshin carbonatites.

Hydrous saline fluids—the probable agents of metasomatism—can form due to immiscibility with carbonatitic magmas (Newton & Manning, 2002, 2010) or as the end products of fractional crystallization (Anenburg et al., 2020). Fluid inclusions in carbonatites are evidence of these fluids in subvolcanic settings (Morogan & Lindblom, 1995; Rankin & Le Bas, 1974; Walter et al., 2020). Khanneshin lava geochemistry indicates that brine activity—recorded by Tl isotopic and La/Yb fractionation—coincided with igneous differentiation from sövite (low REE) to ankerite-barite carbonatite (high REE) compositions that were increasingly hydrous (e.g., Prokopyev et al., 2016). A two-component system (magma-brine and immiscible CO_2-H_2O fluid) may have persisted throughout the differentiation process as the magma evolved to increasingly brine-like compositions. However, this scenario is difficult to reconcile with the evidence for brine-related metasomatism (recorded by Tl isotopes) during early stages of igneous differentiation (manifest as REE enrichment). Instead, we envisage a three-component system—carbonatitic magma, immiscible brine, and immiscible CO_2-H_2O-rich fluid—during igneous differentiation. H_2O solubility in carbonatitic magmas is strongly pressure dependent (Keppler, 2003), which can explain the origins of an H_2O-rich immiscible fluid during magma ascent. Hydrous fluids in equilibrium with carbonatitic magmas become enriched in Na relative to Mg and Ca (Veksler & Keppler, 2000), so H_2O exsolution leads to immiscible brine formation.

Progressively heavier $\delta^{13}C$ in Khanneshin lavas and in carbonatites globally testify to the involvement of CO_2-rich fluids. There are two possible sources of CO_2 in carbonatitic systems. First, decarbonation reactions between carbonate-bearing fluids (magma or brine) and silicate minerals consume the cations in carbonate species and produce CO_2 (e.g., Anenburg & Mavrogenes, 2018). Fenitization is one example, but decarbonation reactions can also occur in the mantle. Second, exsolution of dissolved CO_2 species from carbonatitic magmas may produce CO_2. Jacobson et al. (2020) show that high H_2O solubility in carbonatite magmas is linked to the presence of fluorine—Ol Doinyo Lengai lavas have up to 8 wt% fluorine—possibly via the reactions:

$$H_2O + CO_3^{2-} = 2OH^- + CO_2$$
$$CO_2 + F^- = CO_2F^- \text{(fluoroformate)}$$

The existence of fluoroformate is consistent with Raman spectroscopy of high-pressure molten carbonates (Williams & Knittle, 2003) and implies even higher H_2O solubilities than measured in fluorine-free carbonatite experiments (Keppler, 2003). If so, CO_2 and H_2O may have similar solubilities in carbonatitic magma. Exsolution of H_2O and CO_2 in similar molar proportions from ascending magmas might explain the consistency of $\delta^{13}C$ and $\delta^{18}O$ fractionation patterns among carbonatites globally, which often fit Rayleigh fractionation models with initial H_2O/CO_2 ratios of ~1.

As suggested by Newton & Manning (2002), hydrous saline fluids derived from magmas may become immiscible with CO_2-rich fluids. In ternary NaCl-H_2O-CO_2 systems, hydrous brines are immiscible with CO_2-rich fluids at high temperatures (Aranovich et al., 2010; Liebscher, 2010). This miscibility gap grows with decreasing pressure (Gibert et al., 1998), so the immiscible components (NaCl-H_2O brine and CO_2-H_2O fluid) become increasingly pure as they ascend. $\delta^{18}O$-$\delta^{13}C$ systematics of carbonatites globally suggest that, by the time carbonatitic fluids reach the surface, CO_2 and H_2O exist in approximately equal proportions in exsolved fluids. As our Khanneshin results demonstrate, the high volatile element contents of primary carbonatitic magmas, their rapid ascent, and the miscibility gaps between various fluid components generate dynamic multifluid volcanic systems that are highly reactive with the surrounding silicate wall rock.

Approximately 20% of carbonatite complexes worldwide are associated with micaceous fenites referred to as glimmerites (Elliott et al., 2018). Metasomatic fenite aureoles form around carbonatite complexes (Elliott et al., 2018) and gradually transition into country rock (e.g., Mt Weld, Australia: Lottermoser, 1990). Although such field relations do not exist at Khanneshin volcano, the abundant micaceous xenoliths in

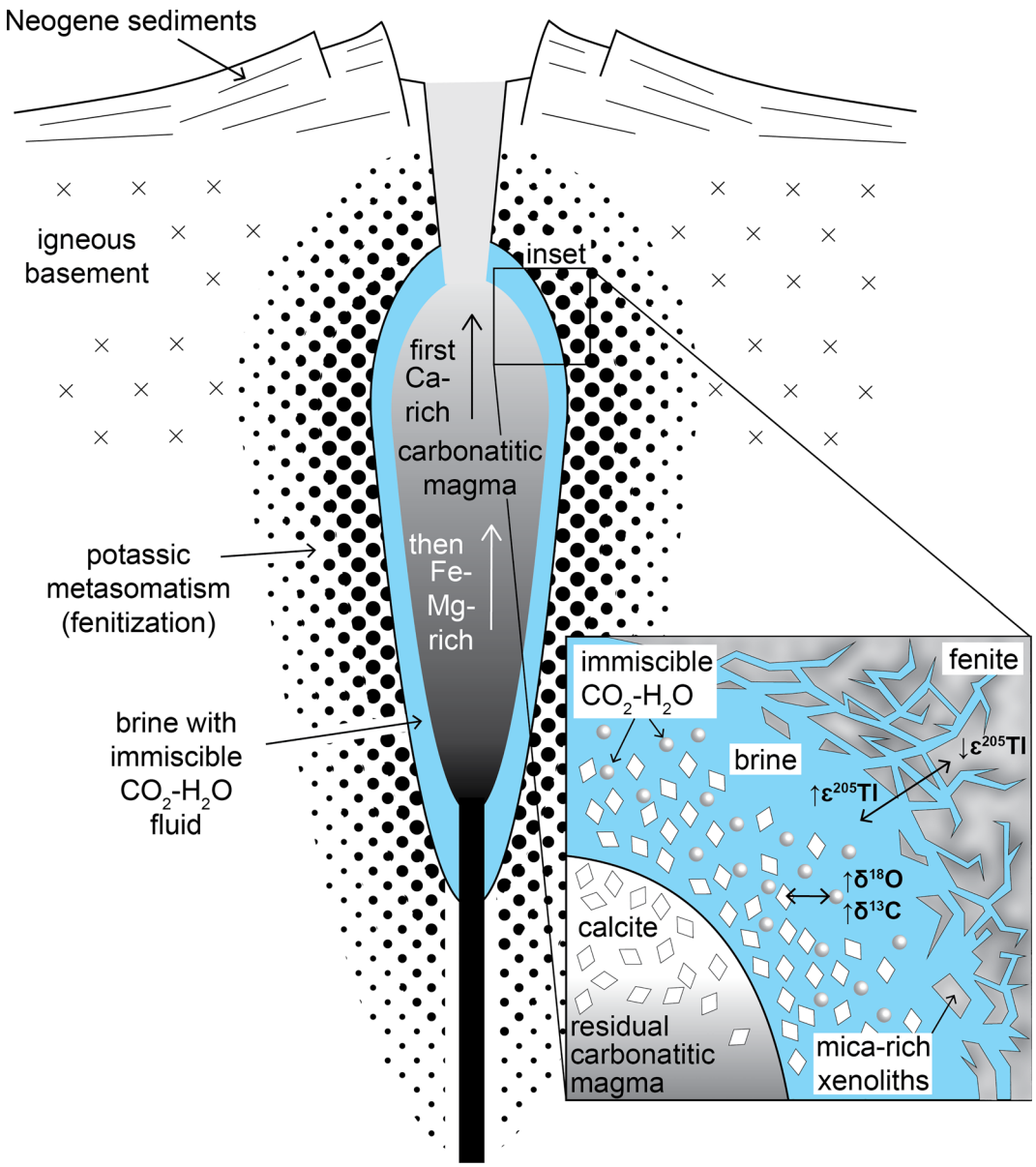

Figure 9. Schematic illustration of the magmatic conduit beneath Khanneshin volcano. We infer that ascending carbonatitic melts exsolved brine that metasomatized the surrounding brecciated wall rock (presumably igneous basement rock underlying the Neogene sedimentary rock), forming a fenite aureole. Fractional crystallization of calcite increased the REE concentrations in the residual magma, which formed ankerite-barite carbonatites. Calcite precipitation from—or in equilibrium with—a CO_2-H_2O-rich fluid component that was immiscible with the brine increased $\delta^{13}C$ and $\delta^{18}O$. Simultaneously, isotopic fractionation associated with metasomatic biotite growth increased the $\varepsilon^{205}Tl$ in the magma-brine system. Double arrows indicate isotopic exchange between two phases. Inspired by Elliott et al. (2018).

Khanneshin lavas are likely wall rock fragments from an analogous subsurface potassic fenite zone. The important role of biotite formation during metasomatism (e.g., Giebel et al., 2019) is highlighted by the Tl isotopic fractionation trend measured in Khanneshin rocks. Although $\varepsilon^{205}Tl$-$\delta^{18}O$ relations temporally link potassic metasomatism (biotite formation) with isotopic exchange between carbonate minerals and CO_2-rich fluids, metasomatizing hydrous brines are probably immiscible with CO_2-rich fluid components under these conditions. Biotite precipitation likely has a negligible effect on the $\delta^{18}O$ and no effect on $\delta^{13}C$ because carbonatite magma-fluid systems dominantly produced carbonate minerals. Tl behaves like K in hydrother-

mal systems (Metz & Trefry, 2000; Nielsen, Rehkämper, Teagle, et al., 2006) and is probably concentrated in hydrous brine that induces metasomatic biotite precipitation, causing the Tl isotope fractionation observed in Khanneshin rocks. Concurrent incompatible element enrichment and Tl isotope fractionation in Khanneshin lavas implies that fenitization occurs in close proximity and association with igneous differentiation (Figure 9), rather than after pulses of expelled fluid leave the magmatic system (e.g., Elliott et al., 2018).

We conclude that the ε^{205}Tl variations of Khanneshin rocks do not reflect primary magma compositions, which were probably isotopically homogenous based on radiogenic isotope measurements (Ayuso et al., 2013). Fenite metasomatism led to progressively heavier ε^{205}Tl values in residual magmas and fluids, so the primary magmas probably had ε^{205}Tl less than −4.6, which was equal to the least evolved carbonatite. This value is significantly lighter than the average upper mantle ($\varepsilon^{205}\text{Tl} = -2 \pm 1$: Nielsen, Rehkämper, Norman, et al., 2006), but is within the range found in low-temperature altered oceanic crust (average $\varepsilon^{205}\text{Tl} \sim -8$: Nielsen, Rehkämper, & Prytulak, 2017) and ocean island basalts with recycled altered oceanic crust components (Blusztajn et al., 2018). Such light values can also be found in organic carbon-rich marine sediments deposited in anoxic environments such as oxygen minimum zones (Owens et al., 2017), but are otherwise uncommon in major terrestrial geochemical reservoirs. If the Tl in Khanneshin carbonatites were derived from either of these two sources, then crustal Tl must have been recycled to the carbonatite source region, probably via subduction given that both low-T altered oceanic crust and anoxic marine sediments form near the seafloor. Subduction of low-T altered oceanic crust and/or marine sediments might also have delivered substantial amounts of crustal carbon into the carbonatite source region. Thus, Tl isotopes may be a powerful tool for tracking recycled components in carbonates worldwide when paired with other stable isotope and trace element geochemical techniques.

5. Conclusions

We observe systematic ε^{205}Tl, δ^{13}C, δ^{18}O, and REE trends in Khanneshin carbonatites that underscore the geochemical role of H_2O- and CO_2-rich fluids in carbonatitic magmatic systems. Simultaneous fractional crystallization of carbonate minerals and potassic metasomatism of wall rock can explain REE enrichment, progressively heavier isotopic ratios (in ε^{205}Tl, δ^{13}C, and δ^{18}O systems), and increasing LREE/HREE in the residual liquids. Similar ^{13}C, ^{18}O, and REE enrichment trends are observed in carbonatite complexes worldwide; ε^{205}Tl systematics link these trends to fenite metasomatism of wall rock by brines. Primary Khanneshin magmas probably ascended from the mantle with ε^{205}Tl lower than typical igneous rocks, so this study highlights the likelihood that crustal recycling processes play an important role in the formation of carbonatitic magmas in the mantle. Khanneshin carbonatites also provide a valuable example of how Tl isotopes can be fractionated in high-temperature environments.

Data Availability Statement

All data are included in the manuscript are publicly available through the EarthChem database (<https://doi.org/10.26022/IEDA/111844>). Detailed reviews from Michael Anenburg, Paolo Sossi, and Angus Fitzpayne improved this manuscript considerably.

Acknowledgements
The authors thank the U.S. Geological Survey for providing access to the Khanneshin samples. This project was supported by funding from Woods Hole Oceanographic Institution Independent Research & Development funds and the National Science Foundation (Award #1911699).

References

Alkhazov, V. Y., Atakishiyev, Z. M., & Azimi, N. A. (1978). Geology and mineral resources of the early Quaternary Khanneshin carbonatite volcano (southern Afghanistan). *International Geology Review*, *20*, 281–285.

Amsellem, E., Moynier, F., Bertrand, H., Bouyon, A., Mata, J., Tappe, S., & Day, J. M. (2020). Calcium isotopic evidence for the mantle sources of carbonatites. *Science Advances*, *6*, eaba3269.

Andersen, A. K., Clark, J. G., Larson, P. B., & Donovan, J. J. (2017). REE fractionation, mineral speciation, and supergene enrichment of the Bear Lodge carbonatites. *Wyoming, USA: Ore Geology Reviews*, *89*, 780–807.

Anenburg, M., & Mavrogenes, J. A. (2018). Carbonatitic versus hydrothermal origin for fluorapatite REE-Th deposits: Experimental study of REE transport and crustal "antiskarn" metasomatism. *American Journal of Science*, *318*, 335–366.

Anenburg, M., Mavrogenes, J. A., Frigo, C., & Wall, F. (2020). Rare earth element mobility in and around carbonatites controlled by sodium, potassium, and silica. *Science Advances*, *6*, eabb6570. https://doi.org/10.1126/sciadv.abb6570

Aranovich, L. Y., Zakirov, I. V., Sretenskaya, N. G., & Gerya, T. V. (2010). Ternary system H_2O-CO_2-NaCl at high T-P parameters: An empirical mixing model. *Geochemistry International*, *48*, 446–455.

Araujo, D. P., Gaspar, J. C., & Garg, V. K. 1998. *The complete phlogopite-tetraferriphlogopite series in the Catalão-I and-II carbonatite complexes, Brazil*. In International Kimberlite Conference: Extended Abstracts (Vol. 7, p. 29–31).

Ayuso, R., Tucker, R., Peters, S., Foley, N., Jackson, J., Robinson, S., & Bove, M. (2013). Preliminary radiogenic isotope study on the origin of the Khanneshin carbonatite complex, Helmand Province, Afghanistan. *Journal of Geochemical Exploration*, *133*, 6–14.

Baker, R. G. A., Rehkämper, M., Hinkley, T. K., Nielsen, S. G., & Toutain, J. P. (2009). Investigation of thallium fluxes from subaerial volcanism—Implications for the present and past mass balance of thallium in the oceans. *Geochimica et Cosmochimica Acta*, *73*, 6340–6359. https://doi.org/10.1016/j.gca.2009.07.014

Bell, K., & Simonetti, A. (2010). Source of parental melts to carbonatites–critical isotopic constraints. *Mineralogy and Petrology*, *98*, 77–89.

Blusztajn, J., Nielsen, S. G., Marschall, H. R., Shu, Y., Ostrander, C. M., & Hanyu, T. (2018). Thallium isotope systematics in volcanic rocks from St. Helena—Constraints on the origin of the HIMU reservoir. *Chemical Geology*, *476*, 292–301. https://doi.org/10.1016/j.chemgeo.2017.11.025

Chakhmouradian, A. R., Reguir, E. P., Couëslan, C., & Yang, P. (2016). Calcite and dolomite in intrusive carbonatites. II. *Trace-Element Variations: Mineralogy and Petrology*, *110*, 361–377.

Dasgupta, R. (2013). Ingassing, storage, and outgassing of terrestrial carbon through geologic time. *Reviews in Mineralogy and Geochemistry*, *75*, 183–229.

Dawson, J. B., Pinkerton, H., Norton, G. E., & Pyle, D. M. (1990). Physicochemical properties of alkali carbonatite lavas: Data from the 1988 eruption of Oldoinyo Lengai, Tanzania. *Geology*, *18*, 260–263.

Deines, P., & Gold, D. P., 1973. The isotopic composition of carbonatite and kimberlite carbonates and their bearing on the isotopic composition of deep-seated carbon. *Geochimica et Cosmochimica Acta*, *37*, 1709–1733.

Elliott, H. A. L., Wall, F., Chakhmouradian, A. R., Siegfried, P. R., Dahlgren, S., Weatherley, S., et al. (2018). Fenites associated with carbonatite complexes: A review. *Ore Geology Reviews*, *93*, 38–59. https://doi.org/10.1016/j.oregeorev.2017.12.003

Falloon, T. J., & Green, D. H. (1990). Solidus of carbonated fertile peridotite under fluid-saturated conditions. *Geology*, *18*, 195–199. https://doi.org/10.1130/0091-7613(1990)018<0195:SOCFPU>2.3.CO;2

Fosu, B. R., Ghosh, P., & Viladkar, S. G. (2020). Clumped isotope geochemistry of carbonatites in the north-western Deccan igneous province: Aspects of evolution, post-depositional alteration and mineralisation. *Geochimica et Cosmochimica Acta*, *274*, 118–135.

Gibert, F., Guillaume, D., & Laporte, D. (1998). Importance of fluid immiscibility in the H_2O-NaCl-CO_2 system and selective CO_2 entrapment in granulites; experimental phase diagram at 5–7 kbar, 900°C and wetting textures. *European Journal of Mineralogy*, *10*, 1109–1123.

Giebel, R. J., Parsapoor, A., Walter, B. F., Braunger, S., Marks, M. A. W., Wenzel, T., & Markl, G. (2019). Evidence for magma–wall rock interaction in carbonatites from the Kaiserstuhl Volcanic complex (Southwest Germany). *Journal of Petrology*, *60*, 1163–1194.

Gittins, J. (1988). The origin of carbonatites. *Nature*, *335*, 295–296. https://doi.org/10.1038/335295a0

Hamilton, D. L., Freestone, I. C., Dawson, J. B., & Donaldson, C. H. (1979). Origin of carbonatites by liquid immiscibility. *Nature*, *279*, 52–54.

Hammouda, T., & Keshav, S. (2015). Melting in the mantle in the presence of carbon: Review of experiments and discussion on the origin of carbonatites. *Chemical Geology*, *418*, 171–188.

Hans Wedepohl, K. (1995). The composition of the continental crust. *Geochimica et Cosmochimica Acta*, *59*, 1217–1232. https://doi.org/10.1016/0016-7037(95)00038-2

Harmon, R. S., & Hoefs, J. (1995). Oxygen isotope heterogeneity of the mantle deduced from global 18O systematics of basalts from different geotectonic settings. *Contributions to Mineralogy and Petrology*, *120*, 95–114.

Haynes, E. A., Moecher, D. P., & Spicuzza, M. J. (2003). Oxygen isotope composition of carbonates, silicates, and oxides in selected carbonatites: constraints on crystallization temperatures of carbonatite magmas. *Chemical Geology*, *193*, 43–57. https://doi.org/10.1016/S0009-2541(02)00244-9

Hulett, S. R., Simonetti, A., Rasbury, E. T., & Hemming, N. G. (2016). Recycling of subducted crustal components into carbonatite melts revealed by boron isotopes. *Nature Geoscience*, *9*, 904.

Jackson, M. G., Hart, S. R., Koppers, A. A. P., Staudigel, H., Konter, J., Blusztajn, J., et al. (2007). The return of subducted continental crust in Samoan lavas. *Nature*, *448*, 684–687. https://doi.org/10.1038/nature06048

Jacobson, N. S., Fegley, B., Setlock, J. A., & Costa, G. (2020). Solubility of Water in Carbonatites. *ACS Earth and Space Chemistry*, *4*, 2144–2152. https://doi.org/10.1021/acsearthspacechem.0c00222

Javoy, M., Pineau, F., & Delorme, H. (1986). Carbon and nitrogen isotopes in the mantle. *Chemical Geology*, *57*, 41–62. https://doi.org/10.1016/0009-2541(86)90093-8

Johnson, D. M., Hooper, P. R., & Conrey, R. M. (1999). *XRF analysis of rocks and minerals for major and trace elements on a single low dilution Li-tetraborate fused bead*. JCPDS-international center for diffraction data.

Keller, J., & Hoefs, J. (1995). *Stable isotope characteristics of recent natrocarbonatites from Oldoinyo Lengai*. Carbonatite volcanism (pp. 113–123), Springer.

Keppler, H. (2003). Water solubility in carbonatite melts. *American Mineralogist*, *88*, 1822–1824.

Kramm, U., & Sindern, S. (1998). Nd and Sr isotope signatures of fenites from Oldoinyo Lengai, Tanzania, and the genetic relationships between nephelinites, phonolites and carbonatites. *Journal of Petrology*, *39*, 1997–2004.

Lee, M. J., Garcia, D., Moutte, J., & Lee, J. I. (2003). Phlogopite and tetraferriphlogopite from phoscorite and carbonatite associations in the Sokli massif, Northern Finland. *Geosciences Journal*, *7*, 9.

Liebscher, A. (2010). Aqueous fluids at elevated pressure and temperature. *Geofluids*, *10*, 3–19. https://doi.org/10.1111/j.1468-8123.2010.00293.x

Lottermoser, B. G. (1990). Rare-earth element mineralisation within the Mt. Weld carbonatite laterite. *Western Australia: Lithos*, *24*, 151–167. https://doi.org/10.1016/0024-4937(90)90022-S

Metz, S., & Trefry, J. H. (2000). Chemical and mineralogical influences on concentrations of trace metals in hydrothermal fluids. *Geochimica et Cosmochimica Acta*, *64*, 2267–2279. https://doi.org/10.1016/S0016-7037(00)00354-9

Morogan, V., & Lindblom, S. (1995). Volatiles associated with the alkaline-carbonatite magmatism at Alnö, Sweden: A study of fluid and solid inclusions in minerals from the La\aangarsholmen ring complex. *Contributions to Mineralogy and Petrology*, *122*, 262–274.

Newton, R. C., & Manning, C. E. (2002). Experimental determination of calcite solubility in H_2O-NaCl solutions at deep crust/upper mantle pressures and temperatures: Implications for metasomatic processes in shear zones. *American Mineralogist*, *87*, 1401–1409.

Newton, R. C., & Manning, C. E. (2010). Role of saline fluids in deep-crustal and upper-mantle metasomatism: Insights from experimental studies. *Geofluids*, *10*, 58–72.

Nielsen, S. G., Klein, F., Kading, T., Blusztajn, J., & Wickham, K. (2015). Thallium as a tracer of fluid–rock interaction in the shallow Mariana forearc. *Earth and Planetary Science Letters*, *430*, 416–426.
Nielsen, S. G., Prytulak, J., Blusztajn, J., Shu, Y., Auro, M., Regelous, M., & Walker, J. (2017). Thallium isotopes as tracers of recycled materials in subduction zones: Review and new data for lavas from Tonga-Kermadec and Central America: *Journal of Volcanology and Geothermal Research*, *339*, 23–40.
Nielsen, S. G., Rehkämper, M., Baker, J., & Halliday, A. N. (2004). The precise and accurate determination of thallium isotope compositions and concentrations for water samples by MC-ICPMS. *Chemical Geology*, *204*, 109–124.
Nielsen, S. G., Rehkämper, M., Brandon, A. D., Norman, M. D., Turner, S., & O'Reilly, S. Y. (2007). Thallium isotopes in Iceland and Azores lavas—Implications for the role of altered crust and mantle geochemistry. *Earth and Planetary Science Letters*, *264*, 332–345.
Nielsen, S. G., Rehkämper, M., Norman, M. D., Halliday, A. N., & Harrison, D. (2006). Thallium isotopic evidence for ferromanganese sediments in the mantle source of Hawaiian basalts. *Nature*, *439*, 314–317.
Nielsen, S. G., Rehkämper, M., & Prytulak, J. (2017). Investigation and application of thallium isotope fractionation: *Reviews in Mineralogy and Geochemistry*, *82*, 759–798.
Nielsen, S. G., Rehkämper, M., Teagle, D. A., Butterfield, D. A., Alt, J. C., & Halliday, A. N. (2006). Hydrothermal fluid fluxes calculated from the isotopic mass balance of thallium in the ocean crust. *Earth and Planetary Science Letters*, *251*, 120–133.
Nielsen, S. G., Wasylenki, L. E., Rehkämper, M., Peacock, C. L., Xue, Z., & Moon, E. M. (2013). Towards an understanding of thallium isotope fractionation during adsorption to manganese oxides. *Geochimica et Cosmochimica Acta*, *117*, 252–265. https://doi.org/10.1016/j.gca.2013.05.004
Nielsen, S. G., Yogodzinski, G., Prytulak, J., Plank, T., Kay, S. M., Kay, R. W., et al. (2016). Tracking along-arc sediment inputs to the Aleutian arc using thallium isotopes. *Geochimica et Cosmochimica Acta*, *181*, 217–237.
O'Neill, H. S. C. (2016). The smoothness and shapes of chondrite-normalized rare earth element patterns in basalts. *Journal of Petrology*, *57*, 1463–1508. https://doi.org/10.1093/petrology/egw047
Ostrander, C. M., Owens, J. D., & Nielsen, S. G. (2017). Constraining the rate of oceanic deoxygenation leading up to a Cretaceous Oceanic Anoxic Event (OAE-2∼ 94 Ma): *Science advances*, *3*, e1701020.
Owens, J. D., Nielsen, S. G., Horner, T. J., Ostrander, C. M., & Peterson, L. C. (2017). Thallium-isotopic compositions of euxinic sediments as a proxy for global manganese-oxide burial. *Geochimica et Cosmochimica Acta*, *213*, 291–307.
Pineau, F., Javoy, M., & Allegre, C. J. (1973). Etude systematique des isotopes de l'oxygene, du carbone et du strontium dans les carbonatites. *Geochimica et Cosmochimica Acta*, *37*, 2363–2377.
Prokopyev, I. R., Borisenko, A. S., Borovikov, A. A., & Pavlova, G. G. (2016). Origin of REE-rich ferrocarbonatites in southern Siberia (Russia): Implications based on melt and fluid inclusions. *Mineralogy and Petrology*, *110*, 845–859.
Rader, S. T., Mazdab, F. K., & Barton, M. D. (2018). Mineralogical thallium geochemistry and isotope variations from igneous, metamorphic, and metasomatic systems. *Geochimica et Cosmochimica Acta*, *243*, 42–65.
Rankin, A. H., & Le Bas, M. J. (1974). Nahcolite (NaHCO 3) in inclusions in apatites from some E. African ijolites and carbonatites. *Mineralogical Magazine*, *39*, 564–570.
Ray, J. S., & Ramesh, R. (2000). Rayleigh fractionation of stable isotopes from a multicomponent source. *Geochimica et Cosmochimica Acta*, *64*, 299–306.
Richet, P., Bottinga, Y., & Javoy, M. (1977). A review of hydrogen, carbon, nitrogen, oxygen, sulphur, and chlorine stable isotope fractionation among gaseous molecules. *Annual Review of Earth and Planetary Sciences*, *5*, 65–110.
Ritter, X., Sanchez-Valle, C., Sator, N., Desmaele, E., Guignot, N., King, A., et al. (2020). Density of hydrous carbonate melts under pressure, compressibility of volatiles and implications for carbonate melt mobility in the upper mantle. *Earth and Planetary Science Letters*, *533*, 116043.
Rubie, D. C., & Gunter, W. D. (1983). The role of speciation in alkaline igneous fluids during fenite metasomatism. *Contributions to Mineralogy and Petrology*, *82*, 165–175.
Santos, R. V. (1995) Variations of oxygen and carbon isotopes in carbonatites: A study of Brazilian alkaline complexes. *Geochimica et Cosmochimica Acta*, *59*, 1339–1352.
Scheele, N., & Hoefs, J. (1992). Carbon isotope fractionation between calcite, graphite and CO_2: An experimental study. *Contributions to Mineralogy and Petrology*, *112*, 35–45.
Spandler, C., & Pirard, C. (2013). Element recycling from subducting slabs to arc crust. *A review: Lithos*, *170*, 208–223.
Taylor, H. P., Jr, Frechen, J., & Degens, E. T. (1967). Oxygen and carbon isotope studies of carbonatites from the Laacher See District, West Germany and the Alnö District, Sweden. *Geochimica et Cosmochimica Acta*, *31*, 407–430.
Thompson, R., Smith, P., Gibson, S., Mattey, D., & Dickin, A., (2002). Ankerite carbonatite from Swartbooisdrif, Namibia: The first evidence for magmatic ferrocarbonatite. *Contributions to Mineralogy and Petrology*, *143*, 377–396. https://doi.org/10.1007/s00410-002-0350-0
Tucker, R. D., Belkin, H. E., Schulz, K. J., Peters, S. G., & Buttleman, K. P. (2011). *Rare earth element mineralogy, geochemistry, and preliminary resource assessment of the Khanneshin carbonatite complex, Helmand Province, Afghanistan*: U.S. Geological Survey Open-File Report.
Tucker, R. D., Belkin, H. E., Schulz, K. J., Peters, S. G., Horton, F., Buttleman, K., & Scott, E. R. (2012). A major light rare-earth element (LREE) resource in the Khanneshin carbonatite complex. *Southern Afghanistan: Economic Geology*, *107*, 197–208.
Veksler, I. V., & Keppler, H. (2000). Partitioning of Mg, Ca, and Na between carbonatite melt and hydrous fluid at 0.1–0.2GPa. *Contributions to Mineralogy and Petrology*, *138*, 27–34.
Vikhter, B. Y., Yeremenko, G. K., & Chmyrev, V. M. (1976). A young volcanogenic carbonatite complex in Afghanistan: *International Geology Review*, *18*, 1305–1312.
Walter, B. F., Steele-MacInnis, M., Giebel, R. J., Marks, M. A. W., & Markl, G. (2020). Complex carbonate-sulfate brines in fluid inclusions from carbonatites: Estimating compositions in the system H_2O-Na-K-CO_3-SO_4-Cl. *Geochimica et Cosmochimica Acta*, *277*, 224–242. https://doi.org/10.1016/j.gca.2020.03.030
Weidendorfer, D., Schmidt, M. W., & Mattsson, H. B. (2016). Fractional crystallization of Si-undersaturated alkaline magmas leading to unmixing of carbonatites on Brava Island (Cape Verde) and a general model of carbonatite genesis in alkaline magma suites. *Contributions to Mineralogy and Petrology*, *171*, 43.
Williams, Q., & Knittle, E. (2003). Structural complexity in carbonatite liquid at high pressures. *Geophysical Research Letters*, *30*, 1022. https://doi.org/10.1029/2001GL013876
Woolley, A. R. (1982). A discussion of carbonatite evolution and nomenclature, and the generation of sodic and potassic fenites. *Mineralogical Magazine*, *46*, 13–17.
Woolley, A. R., & Church, A. A. (2005). Extrusive carbonatites: A brief review. *Lithos*, *85*, 1–14.

Workman, R. K., Eiler, J. M., Hart, S. R., & Jackson, M. G. (2008). Oxygen isotopes in Samoan lavas: Confirmation of continent recycling. *Geology*, *36*, 551–554.

Wyllie, P. J. (1989). Origin of carbonatites: Evidence from phase equilibrium studies. In K. Bell (Ed.), *Carbonatites: Genesis and evolution* (pp. 500–545). London: Unwin Hyman. Retirved from https://resolver.caltech.edu/CaltechAUTHORS:20160224-152118970

Wyllie, P. J., & Huang, W.-L. (1975). Peridotite, kimberlite, and carbonatite explained in the system CaO-MgO-SiO_2-CO_2. *Geology*, *3*, 621–624. https://doi.org/10.1130/0091-7613(1975)3<621:PKACEI>2.0.CO;2

Yeremenko, G. K., Vikhter, B. Y., Chmyrev, V. M., & Khabibulla, K. (1975). Quaternary volcanic carbonatite complex in Afghanistan, in Doklady Academy of Science, USSR. *Earth Science Section*, *223*, 53–55.

Zindler, A., & Hart, S. (1986). *Chemical geodynamics. Annual review of earth and planetary sciences* (Vol. 14, pp. 493–571).